Ludwig-Maximilians-Universität
München Fakultät für
Geowissenschaften Department für
Geographie

MASTERARBEIT
Umweltsysteme und Nachhaltigkeit
Monitoring, Modellierung und
Management

Wissenschaftliche Arbeit zur Erlangung des akademischen Grades Master of Science

LiDAR-Based Assessment of Microtopography on Seismic Lines in Northern Alberta´s Boreal Forest

Betreuer:
Prof. Dr. Ralf Ludwig

Mitbetreuung:
Prof. Dr. Scott Ketcheson
(University of Athabasca)

Verfasser:
Jasper
Koch
Waldfriedhofstraße 105,
81377 München
jasper.koch@campus.lmu.de

Acknowledgments

I am profoundly grateful to Professor Dr. Ralf Ludwig for providing me with this extraordinary opportunity to conduct fascinating research in the boreal forests of Canada. This opportunity had a significantly positive impact on my memories of my master's program, particularly following the COVID-19 period.

Special appreciation goes to Professor Dr. Scott Ketcheson for welcoming me into his wonderful lab of hardened field researchers and helping me explore the beautiful, dirty, tough, rewarding and adventurous world of peatland science. As well as mentoring me through the long process of writing this thesis. I would also like to thank Professor Dr. Greg McDermid for letting me be part of his lab and giving me much valuable insight into the fascinating RPAS world. As well as allowing me to use all your valuable and fragile equipment.

Special thanks also to Dr. Julia Linke for organizing so much of this stay. I am grateful to Maverick Fong for his assistance in resolving numerous GNSS issues, Dr. Richard Zeng for his technical expertise, Xue Yan for inspiring days of fieldwork and piloting skills and Sean Hillson for his support through long but entertaining field days. I would like to extend my gratitude to the Mitacs Globalink Research Award, the BERA project, the University of Calgary, and the Ludwig-Maximilians-University (LMU) Munich. Their financial support made this opportunity possible and played a pivotal role in the realization of this thesis.

Many thanks also to Lelia and Joe for supporting me in the field, being good friends and never dropping me during our climbing sessions. Irina and Tony for all the fun moments in the mountains, the delicious steaks and your general support. I also wish to express my appreciation to Marlis, for her assistance with the LiDAR workflow, Patrick for being a good roommate and Niklas for always keeping me up to speed. The time spent with all of you during our stay was truly memorable.

A special note of thanks to my parents for their encouragement and support throughout this process.

Last but not least I want to thank my good friends Adrian, Stefan, my sister Helene and especially Deianira for their feedback and advice. Their support has meant a great deal to me!

Abstract

Abstract

Oil and gas exploration in northern Alberta has led to the creation of dense networks of linear disturbances boreal forest, commonly referred to as seismic lines. The slow regeneration of these clearings has had a number of detrimental ramifications, most prominently the decrease in the woodland caribou population. The variability of microtopography plays a crucial role in the regeneration of seismic lines in wetlands, as small elevations rising above the water table allow seedlings to develop. Therefore, information on the extent of microtopography is highly relevant to the coordination of efforts aiming to restore microtopography. The aim of this study was to develop and validate a workflow that extracts information on microtopography from Light Detection and Ranging (LiDAR) based on Remotely Piloted Aircraft System (RPAS). The analysis of the accuracy of the LiDAR revealed substantial differences in accuracy based on environmental conditions and a RMSE of 20 cm for the entire study area. Aircraft based LiDAR was found to outperform the RPAS LiDAR substantially, achieving a RMSE of 12 cm, indicating that high point density may not be correlated with higher accuracy. The performance of the three microtopography quantification methods, Surface Area Ratio (SAR), Depth-to-Water (DTW) and Microform analysis was found to be dependent on the setting of the environment, and research question. When employed to measure the depression of seismic line disturbance in a poor fen area, all three measured significant differences in the microtopography compared to the undisturbed areas, indicating a slowed regeneration process.

Table of Contents

I. List of Figures

II. List of Tables

III. List of Acronyms

ALS	Airborne Laser Scanning
BERA	Boreal Ecosystem and Recovery Assessment
CAD	Canadian
CNRL	Canadian Natural Resource Limited
DSM	Digital Surface Model
DTM	Digital Terrain Model
DTW	Depth-to-Water
FLM	Forest Line Mapper
GCP	Ground Control Points
GNSS	Global Navigation Satellite System
GWL	Groundwater Level
IMU	Internal Measurements Unit
LiDAR	Light Detection and Ranging
NAD83	North American Datum
NRCan	Natural Resources Canada
RMSE	Root Mean Square Error
RPAS	Remotely piloted Aircraft System
RTK	Real Time Kinematic
SAR	Surface Area Ratio
SfM	Structure from Motion
TIN	Triangulated Irregular Network
TLS	Terrestrial Laser Scanning
TRI	Terrain Ruggedness Index

1 Introduction

The boreal forests of Canada cover roughly 627 million ha, translating to 29% of North America's surface area (excluding Mexico). These forests are home to a large diversity of plants and animals, whilst the exploitation of its resources contribute greatly to the local economy (Brandt et al., 2013). They represent a globally salient carbon sink, as they are home to 28% of the global peatland area, storing ca. 147 billion tonnes of soil carbon (Strack, 2008). The ecology of these peatlands is controlled by a delicate balance of factors such as hydrology, vegetation, chemistry, climate, etc. As a consequence, any disturbances of these factors may lead to the deterioration of the ecological functioning of the peatlands, resulting in a loss of biodiversity and high greenhouse gas emissions (Price et al., 2013; Strack, 2008; Strack et al., 2019).

Alberta currently contains one of the largest petroleum deposits worldwide, which is subject to intensive industrial exploitation. As the oil is bound to sand and spread across a vast area of the boreal forest, the search for oil has resulted in the creation of a dense networks of so-called seismic lines. These are kilometre-long clearings through the forest that serve to transport equipment to locate oil resources with the use of seismic measurements. Alone in Alberta, these seismic lines have a combined estimated length of up to 1,7 Million km. Their influence on their surrounding ecosystems is far-reaching and complex. On many of these lines the vegetation is failing to recover and is stuck in a state of so-called arrested succession (Brandt, 2013). This effect is especially pronounced in wetland areas, as these complex ecosystems present challenging conditions for vegetation regrowth, due to the wet, waterlogged conditions characteristic of these areas (van Rensen et al., 2015).

The persistent presence of these seismic lines has been shown to aid predators by making hunting and traveling easier. This has been implicated in the dwindling population of the woodland caribou (*Rangifer tarandus caribou*), an animal now listed as threatened under the Canadian Species-at-Risk Act (Branch, 2023). Furthermore, these seismic lines also are observed to increase greenhouse gas emissions, thus exacerbating the problem of climate change (Lovitt et al., 2018). In order to counter these problems, a number of initiatives aim to restore seismic lines (Hebblewhite, 2017).

One important variable to determine the likelihood of future recovery of seismic lines in wetland environments, is the level of microtopography. Little elevations called hummocks form elevated platforms over the shallow water table, typically encountered in wetlands areas. These

elevations form important habitats for seedlings, which require a dry setting in order to develop a healthy root structure. Seismic lines with a healthy hummock and hollow microtopography are thus more likely to see further recovery (Lieffers and Rothwell, 1987).

In order to speed up the regeneration process of seismic lines stuck in a state of arrested succession, active restoration treatments, such as artificial mounding are being applied to enhance the level of microtopography (Filicetti et al., 2019). Identifying lines with poor microtopography is therefore highly desirable to efficiently direct future restoration work to areas that would likely benefit from mounding. Previous researchers have measured microtopography using Remotely Piloted Aircraft Systems (RPAS) based photogrammetry. Photogrammetry however is limited in its ability to reliably penetrate the canopy cover of dense vegetation, therefore limiting the accurate capture of complex ground features to open terrain (Lovitt et al., 2017). Lovitt speculated that RPAS based LiDAR sensors with high point densities would be able to reliably penetrate thick canopy cover, which would allow for the extraction of ground features in complex forested sites.

Based on these assumptions this thesis aims (i) to build a LiDAR processing workflow that allows for the generation of high-resolution Digital Terrain Models (DTM) and evaluate the accuracy on a variety of seismic lines. The quality of the RPAS based LiDAR will then be compared to lower resolution aircraft-based LiDAR, to evaluate if measurements of microtopography are scalable to a potentially much larger area. Based on the generated DTMs (ii) different methods of quantifying the microtopography will be evaluated and (iii) applied in a case study on a wetland, to evaluate the effect of seismic lines on the microtopography.

The findings of this research will contribute to the Boreal Ecosystem and Recovery Assessment (BERA) project. The project aims to support ecosystem recovery efforts by enhancing our understanding of the implications of industrial disturbances on natural ecosystem dynamics and formulating strategies for restoration. As part of its resources, the project includes tools such as the Forest Line Mapper (FLM), that map the impact area of seismic lines, as outlined by Queiroz et al., 2020. Ultimately the methods outlined in this thesis are to be integrated into the FLM.

2 Background

Figure 1 Location of the oil sand area in the boreal forest of northern Alberta (Langor, 2015).

2.1 Oil and Gas Exploration in Alberta

Situated in the boreal forests of northern Alberta, the Canadian oil sands are third largest oil deposits worldwide, with some 160 billion barrels of economically recoverable bitumen. As visible in Figure 1, the oil sands lie beneath some 142,200 km2 of Alberta, located in three separate regions; Cold Lake, Peace River and Athabasca (Government of Alberta, 2023) . Open pit mining is one way of accessing the oil sands close to the surface, leading to the complete removal of the boreal forest landscape, permanently altering the ecology of these areas. Although the disturbance created by this practice is extremely disruptive, it tends to be spatially concentrated. In order to access the deeper oil sand deposits, situ methods have to be applied, which rely on the injection of large amounts of hot water vapour to mobilise the viscous bitumen, that can then be pumped to the surface. The necessary infrastructure for these operations (such as access roads, pipelines, well pads and seismic lines) leads to low intensity disturbance spread out over large areas (Johnson and Miyanishi, 2008).

Seismic techniques are required to locate the oil sand deposits. These rely on linear forest clearings that allow for the movements of the equipment and workers. Beginning in the 1950s, these so-called 2D seismic lines were cut using bulldozers clearing 5 to 10 metre wide openings in low density networks covering most of northern Alberta. The density of these lines ranges from 1 km up to 10 km per km^2 in the primary oil producing region around Fort McMurray (Lee and Boutin, 2006). This practice often led to the complete removal of the topsoil, and it became apparent that a method introducing less disturbance was desirable. Starting in the 1990s, a narrower type of seismic lines with a greatly reduced width between 2 and 4 metres emerged. Often referred to as 3D lines or "low impact" seismic lines, these are often employed in much denser networks of up to 40 km of line per km^2. As the practice of in situ oil extraction was expanding, it became evident that frequent seismic surveys would benefit the oil extraction process as the injection of steam could be controlled more efficiently. This led to the practice of 4D seismic lines, meaning that lines are frequently recut to enable new surveys (Stern et al., 2018).

Figure 2 Seismic line located in a peatland in Stony Mountain. Of particular note should be the lack of recovery on the seismic line inside the peatland..

Figure 3 Seismic line intersecting upland ecosites. Notable recovery in some sections.

Initially, it was expected that these seismic lines would regrow and the ecosystems would return to their previous state, but it quickly became obvious that for many seismic lines this recovery would happen at unacceptably long time scales (van Rensen et al., 2015). Whilst many seismic lines experience a period of vegetation regrowth in the beginning, they then often reach a state of arrested succession (as shown in Figure 2 and Figure 3), in which the vegetation struggles to rebound to common recovery criteria. This also applies to the "low impact" seismic lines, where the recovery process has been taking longer than expected (Dabros et al., 2018).

The slow recovery of these linear disturbances is associated with a wide array of problems. The most prominent example is the rapid decline of the woodland caribou *(Rangifer tarandus caribou).* This is largely attributed to the increased line of sight and ease of movements for predators such as wolves (as visible in Figure 4), leading to more caribou falling victim to predation (Latham et al., 2011). Another problem is the increased release of potent greenhouse gases such as CH_4 on seismic lines in peatlands (Strack et al., 2019). Other effects such as the wide spread fragmentation of the boreal forest, leading to a variety of edge effects are not well understood, but are associated with a change in plant compositions of the surrounding forest ecosystem (Dabros et al., 2018; Echiverri et al., 2022).

To understand the slow recovery on seismic lines, the site limiting factors impeding the recovery process must be studied. These include soil compaction from heavy machinery, different microclimatic conditions and increased human access to remote areas, leading to e.g., disturbance by recreational terrain vehicles. Moreover, the challenging climatic conditions in northern Alberta lead to slow overall plant growth, making recovery a slow process (Dabros et al., 2018). One frequently mentioned site limiting factor important to the recovery of seismic lines in peatlands is the level of microtopography (Filicetti et al., 2019; Stevenson et al., 2019).

Figure 4 Wolves patrolling a seismic line.

2.2 Microtopography in Wetlands

The term microtopography describes the variations in surface height occurring in small scales in peatlands (Cresto Aleina et al., 2016).These so-called microforms are often divided into hummocks and hollows. Hummocks describes areas where the growth of sphagnum has accumulated to form a small prominence, while hollows describe the depressed areas separating the hummocks (Holmquist et al., 2014; Strack, 2008). These microforms often occur around the 1x1 metre scale (Cresto Aleina et al., 2015).

The contribution of the different factors responsible for the formation of microforms remains a subject of debate between researchers. Hogg, 1993 suggests that the pattern of microforms is largely driven by the spatial distribution of sphagnum species and inherent variations in their rates of decomposition. Other authors point to local variations in the soil moisture and depth to water table as primary drivers of microform formation (Strack, 2008; Acharya et al., 2015).

The hummocks and hollows have a strong influence on the ecological functioning of peatlands. They greatly affect the local hydrology as a consequence of the improved water retention caused by the microforms slowing down the waterflow and high water holding capacity of sphagnum species (De Roos et al., 2018). Hummocks are especially important for the establishment of seedlings as they provide an important buffer from the high water table in wetlands. This provides the roots more space to grow, offers a favourable moisture environment and provides the seedling a milder microclimate (Lieffers and Rothwell, 1987)

The lack of microtopography on seismic lines has been shown to heavily reduce the establishment of seedlings, and to be one of the major site limiting factors inhibiting recovery (Caners and Lieffers, 2014; Filicetti et al., 2019). Stevenson et al., 2019 measured the microtopography on seismic lines in peatlands to be reduced on average by 8 cm, with strong depressions being observable on lines even decades after their creation. This is linked to a positive feedback loop, whereby the high water table, amongst other factors, inhibits the growth of hummock forming sphagnum species (Caners and Lieffers, 2014).

2.2.1 Mounding

In order to disrupt the positive feedback loop described in chapter 2.2 and to restore the variability of microtopography and accelerate recovery, the practice of creating artificial microtopography by mounding has been established, as visible in Figure 5. Mounding involves the excavation of mineral and organic soil, forming hummocks next to little hollows (Sutton, 1993). These mounds create an enhanced growing site for seedlings, by increasing the potential rooting depth and providing a warmer microclimate (Pyper et al., 2014). Filicetti et al., 2019 measured increased seedling growth and higher survivability of lines treated by mounding, but also found a varying effectiveness of mounding on poor fens. The practice of mounding is very expensive, costing on average 12.500 CAD dollars per km of seismic line, mainly due to the remoteness and narrowness of many lines (Pyper et al., 2014). Mounding also leads to the disturbance of regrown vegetation and is associated with increased greenhouse gas emissions.

This happens as a consequence of exposure of organic mass to aerobic decomposition leading to higher mineralization of carbon, while the open water is associated with higher CH_4 emissions (Schmidt et al., 2022).

Figure 5 A mounded line located parallel to a newly cut line.

It is therefore, highly desirable to apply mounding exclusively to lines that would benefit from a restoration of microtopography. Consequently, measuring the level of microtopography on seismic lines is an important step in order to direct restoration efforts more efficiently. A previous study by Stevenson et al. 2019 used in-situ altimeter measurements to measure seismic line depression. While the altimeter can detect microtopography very accurately, the high quantity of lines make it impractical to apply this method on a large scale.

2.3 Remote Sensing Microtopography

Remote sensing offers a greater scalability of microtopography measurements. Although the resolution of spaceborne sensors is improving, at present they are not good enough to capture the small scale variation found between seismic lines and their surroundings (Lehmann et al., 2016). Therefore, airborne platforms have to be employed. Here the differentiation should be made between piloted aircraft systems and remotely piloted aircraft systems (RPAS).

RPAS systems have the advantage of offering very high spatial and temporal resolution, providing the ability to collect high-quality data, whilst being cost effective compared to piloted systems when smaller areas are surveyed. In general flight campaigns are easy to organise and require comparatively little capital to conduct. On the other hand, the reliance on favourable

weather conditions for flights and image quality can potentially limit their usability in some settings (Fritz et al., 2013). Further, their flight times are limited due to poor battery life, limiting the area they can cover. The payload restrictions on the typically smaller RPAS, limits the type and size of sensors being employed. This can create distortions in the case of the shorter focal length of digital cameras amongst others (Westoby et al., 2012).

Piloted aircraft surveys have the advantage of being able to carry heavy and capable sensor payloads at higher altitudes, which enables the surveying of several thousand square kilometres. Therefore, highly detailed information can be extracted for large areas, enabling better understanding of how ecological dynamics play out throughout on larger scales. Yet, these flight campaigns are usually expensive to conduct and require a lot of planning and resources.

As the monitoring of microtopography is reliant on measuring small variations of the ground surface height, methods that create very accurate digital terrain models (DTM) as output are needed. One method commonly used by researchers is Light Detection and Ranging (LiDAR), which actively sends out and receives electromagnetic radiation. Photogrammetry on the other hand relies only on measuring incoming radiation.

2.3.1 Sensors

As the monitoring of microtopography is reliant on measuring small variations of the ground surface height, methods that create very accurate digital terrain models (DTM) as output are needed. One method commonly used by researchers is Light Detection and Ranging (LiDAR), which actively sends out and receives electromagnetic radiation. Photogrammetry on the other hand relies only on measuring incoming radiation.

2.3.1.1 Photogrammetry

Lovitt, 2017 used Structure from Motion (SfM) photogrammetric models to measure microtopography in peatlands. SfM however relies on Ground Control Points (GCP) to generate spatially correct point clouds. These GCPs have to be placed in the field and the location has to be measured by a Real Time Kinematics (RTK) unit. This process is time consuming and may not always be feasible, especially if data is collected in places with difficult access. Another drawback is that SfM is not good at penetrating thick vegetation. As the technique relies on recording objects from different angles to derive their location, foliage will block access to the ground surface. Therefore, the number of points measured below tree cover will be relatively

low compared to high resolution LiDAR. As a result, the accuracy of digital terrain models derived from SfM is highly dependent on the surface complexity (Westoby et al., 2012). Lovitt et al 2017 concluded that while UAV photogrammetry is generally suitable for characterizing terrain under all but the most heavily vegetated site condition, it is limited in spatial coverage and subject to potential errors from factors such as flight and weather conditions.

2.3.1.2 LiDAR

High resolution LiDAR promises to correct many of the shortcomings of Photogrammetry. LiDAR emits laser pulses and measures the round trip time of the pulse to determine the distance to a reflective object. In combination with global navigation satellite systems (GNSS) and an internal measurements unit (IMU) these systems can produce highly accurate point clouds. As the laser penetrates canopy cover much better than photogrammetric models, high density LiDAR point clouds are able to produce accurate ground information through thick vegetation, making it a very popular system in forest environments (Chisholm et al., 2013; Erdody and Moskal, 2010; Van Rensen et al., 2015). LiDAR does also not rely on preplaced GCPs, making it very useful for producing surface models for large study areas. Newer LiDAR systems are small enough to be fitted to RPAS, enabling very high point densities.

2.3.2 Quantifying Microtopography

2.3.2.1 Moving Window Method

Peatland microtopography, has previously been quantified through terrestrial or aircraft surveys via assessments of topographic features such as relative elevation, slope, vegetation community characteristics, and depth to water table (Bubier et al., 1993; Eppinga et al., 2009; Lehmann et al., 2016). The classification thresholds for these microforms were often based on site-specific surface morphology and researcher subjectivity, with hummocks usually being identified as areas rising 20-50cm above surrounding hollows (Hogg, 1993; Bubier et al., 1993; Pouliot et al., 2011). However, simple elevation thresholds have generally proven to be a simple but effective method for extracting microtopography. Building upon this, Lovitt et al. (2017) implemented a method using a low-pass filter to generate a reference surface, from which a microtopography surface was derived. This surface was then classified using a pixel-based density slicing approach, identifying hummocks, hollows, and trees, based on the assumption that areas taller than the average elevation of the surrounding peatland corresponded with hummocks, while areas below average elevation corresponded with hollows.

Lovitt, 2017 found significant differences between undisturbed and disturbed areas ($p<0.01$), with seismic lines averaging 2.2cm lower than undisturbed peat, and a noticeable overall flattening of microtopographic features along these lines. In contrast, undisturbed areas exhibited more variation in ground-surface elevations, specifically a heightened occurrence of tall hummocks, with ground elevations ranging from -74cm below to +97cm above the reference surface, compared to a range of -64cm to +64cm in disturbed areas. Differences were also observed in the frequency of hummocks versus hollows, with a higher presence of hollows (60.8% coverage) along seismic lines compared to near-equal occurrences in undisturbed areas (51.8% hollow coverage).

2.3.2.2 Depth-to-Water

Another method of quantifying microtopography in wetland areas is the workflow proposed by Rahman et al., 2017, which uses orthophotography and photogrammetric point clouds acquired from RPAS. Their approach leveraged the abundance of surface water pockets in peatlands, which they assumed to be reflective of groundwater level (GWL) in peatlands with high soil conductivity.

The first step of their workflow produced a DSM and a DTM from the photogrammetric point cloud. They then classified surface water using the RPAS-acquired data and extracted a sample of water elevations from these classified areas. Using these samples, they generated continuous models of GWL through interpolation. Maps of depth to water (DTW) were then generated by subtracting their estimates of the GWL with the DTM. Well measurements revealed accuracies in the 20-cm range, though errors were concentrated to upland pockets in the study area, and areas of dense tree covers. Model estimates in the open peatland areas were considerably better. Rahman, 2017, suggested that integrating high-density LiDAR data to the workflow might help to more accurately define terrain in challenging locations.

3 Materials and Methods

3.1 Study Area

All of the study sites are located in northern Alberta in the boreal forest natural subregion and within the Athabasca Oil Sands area (as visible in Figure 6). The study areas is defined by its subartic climate with cold winters and mild to warm summers. Average temperatures range from -17.4°C in January to 17.1°C in July. The annual mean precipitation is 418.6 mm, with most of the precipitation falling in early summer. The main growing season starts in May and lasts until September (Canada, 2013).

In upland regions, the vegetation is often dominated by coniferous trees like Jack Pine (Pinus banksiana), alongside deciduous species such as Aspen (*Populus tremuloides*) and Balsam Poplar (*Populus balsamifera*). In contrast, the wetlands feature Black Spruce (*Picea mariana*) and Tamarack (*Larix laricina*), which are adapted to, wet conditions, along with a variety of sphagnum species. The understory across both areas includes a mix of shrubs, such as Labrador tea, berry-producing plants, and various herbaceous plants and ferns.

The Kirby South site is located 50 km from Lac la Biche and leased by the oil and gas company Canadian Natural Resource Limited (CNRL). Here active extraction of oil sand deposits is going via in-situ methods. Therefore, there are a number of linear disturbances such as mineral filled roads, pipelines and a dense network of seismic lines disrupting the boreal landscape. The 3D network of seismic lines here is also subject to frequent re-disturbance, as extraction processes here are actively monitored.

The Stony Mountain site is situated on a plateau between 600 to 850 metres above sea level. As it dominates the surrounding areas, it is the origin of a number of regional catchments divided by terrain features. Active exploration of oil sand deposits is ongoing, but currently no active extraction is taking place here.

The Surmount site is situated on the eastern slope of Stony Mountain. Here in situ oil sand extraction has been going on since 1997, with many extraction sites having been abandoned. Therefore, there are a lot of older seismic lines here that are in a state of regeneration.

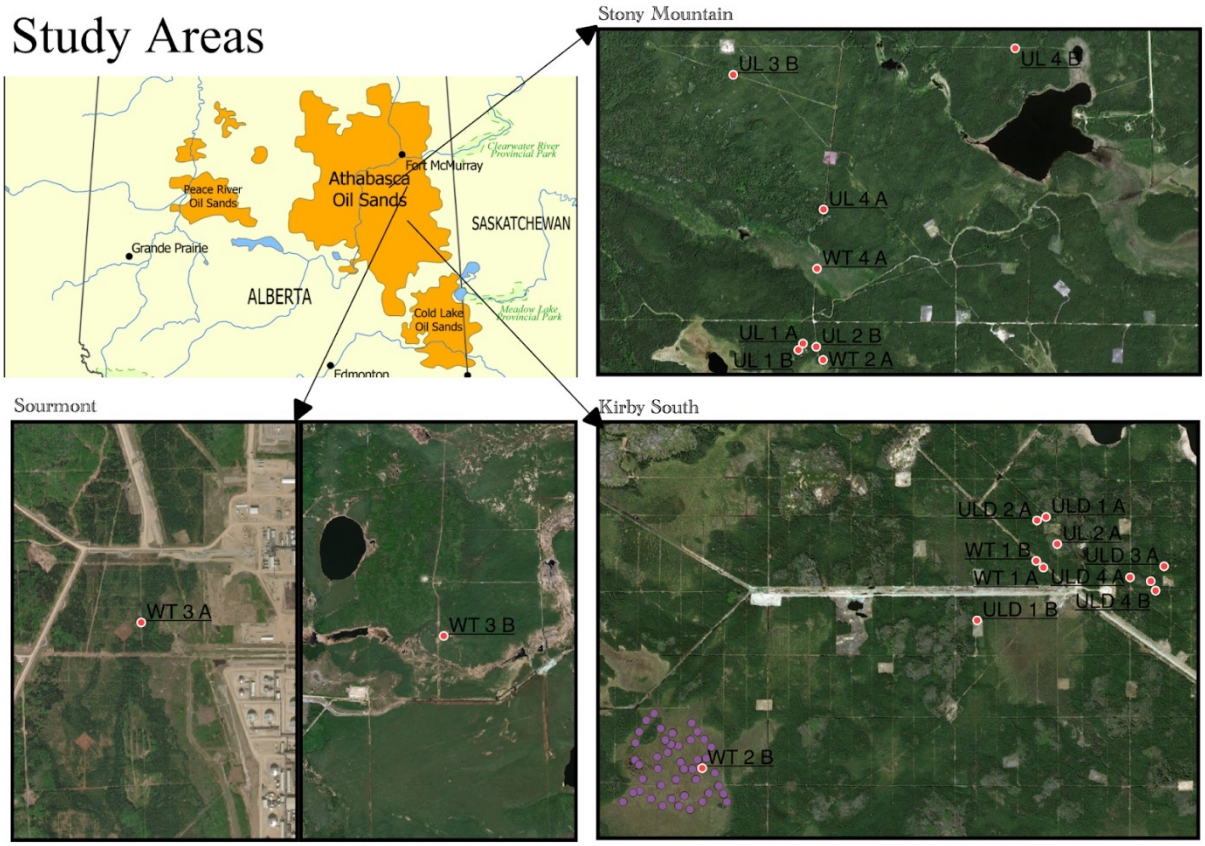

Figure 6 Location of RPAS flights and validation measurements, within the Athabasca region.

3.2 RPAS LiDAR Data Acquisition

3.2.1 Material

The Airborne LiDAR flight campaign was conducted between June and August of 2022. The remotely piloted aircraft system (RPAS) was a DJI Matrice 300 RTK that uses a GNSS ground unit to transmit real time correction data to the RPAS GNSS unit, in a process referred to as real time kinematics (RTK). The LiDAR sensor employed was the DJI Zenmuse L1 Sensor which features an internal IMU unit, that is calibrated during the flight and in combination with the RTK unit allows surface measurements accurate to 10 cm horizontally and 5 cm vertically at a height of 50 meters (DJI, 2022). The laser works at a wavelength of 905 nm, a wavelength suitable for the generation of accurate ground models in vegetated areas (Nelson et al., 2022).

3.2.2 Field Mission

The RPAS field missions were conducted on the 26. and 27-6-2022 in the Stony Mountain, on the 15-7-2022 in Kirby South and on the 4.8.2022 in Surmount. A total of 16 flights were conducted. The changes in vegetation between the flight dates are assumed to be negligible.

The flights were conducted at a height of 100 meters with an overlap of 50 % between flight swaths. The point density per sqm was set at 147 points/m^2.

3.3 GNSS Ground Sampling

3.3.1 Material

In order to evaluate and validate the LiDAR workflow on seismic lines a ground sampling mission using a Real Time Kinematic Global Positioning System (RTK GPS) was conducted over the study areas. The systems used were two Hemisphere S631 GNSS Antennas, that can achieve a Two-Dimensional Root Mean Square 95% confidence accuracy of 15 mm. Per point five GNSS measurements were averaged with the settings on the rover allowing a maximum standard deviation of up to 3 cm between these measurements. This was deemed to be accurate enough for validation measurements, while still allowing RTK measurements under canopy cover where the GNSS signal is more prone to interception by vegetation.

3.3.2 Stratification

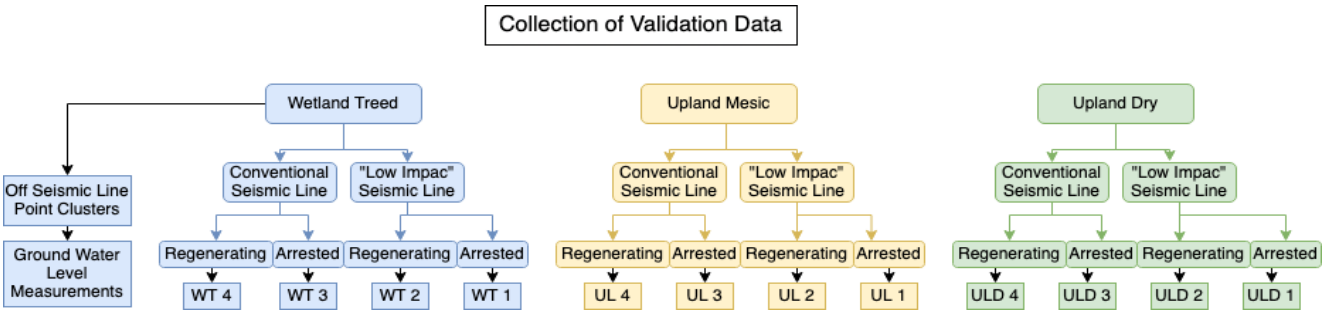

Figure 7 Layout of the stratification of validation measurements.

Figure 7 visualizes the stratification process. In order to gain a comprehensive understanding of the accuracy of LiDAR measurements across the wide variety of seismic lines, a stratification of seismic lines was conducted according to the guidelines of the BERA Strategy Manual, 2022. The validation measurements were conducted in most commonly encountered coarse ecosite types Upland Dry, Upland Mesic and Wetland Treed (examples visible in Figure 8). While Transitional and Wetland Open are left out, as they only cover a small percentage of the BERA study area. The seismic lines in the ecosystems are then differentiated between conventional and “low impact” lines. A further differentiation took place between the lines that are in a state of arrested succession and advanced regeneration, the classification taking place according to the recovery thresholds set by the BERA Manual, 2022. The regeneration on the line was important for the later LiDAR measurements, as vegetation will decrease the accuracy of the

LiDAR microtopography measurements. An additional set of cluster points was measured in a poor fen area, to gain an understanding of accuracy in undisturbed areas. This was done to enable a study comparing microtopography on and off seismic lines.

Figure 8 ***A****: Dry Upland site in a state of arrested succession.* ***B****: Upland Mesic site in state of regeneration.* ***C****: Non-regenerating Wetland site.* ***D****: Wetland site in a state of regeneration.*

3.3.3 Measurements

Per strata class, two sites were selected, in order have a backup site in case measurements were not possible or measurements errors occurred. Per site a total of three transects were conducted. The two outer transects include 30 points per transect spaced in 50 cm increments. The purpose of the outer transects is to give an estimate of the accuracy on the edge line. The inner transects included a total of 60 points with a 25 cm spacing, to allow for a quantification of the microtopographic variability independent of the LiDAR measurements, as described in Chapter 3.5.2. This quantification method followed the methodology of (Stevenson et al., 2019), using a RTK unit instead of an altimeter. In total, some 2492 points were surveyed. To measure the accuracy to the LiDAR outside of seismic lines, a second dataset was created, following the methodology of Lovitt, 2017. This dataset consists of randomly positioned clusters of 5 to 10 points in a fen area in Kirby. For each of these clusters an additional water table measurement was conducted, by measuring the position of the surface water, with the RTK unit. In total 306 points were measured this way.

3.4 LiDAR Processing Workflow

The first steps consisted in processing the raw LiDAR files with the DJI Terra application, in order to transform the Photo/IMU/GNSS/Point cloud data storage and calibration files into the LAS format commonly used to process LiDAR point clouds (Figure 9, a).

For further work the LAStools Software was used, an open-source point cloud processing program with an active user base. LAStools offers a great variety of settings and through multithreading allows efficient processing of large datasets. In the first step the overlapping flightlines were eliminated using LASoverage to get rid of artefacts that would skew the results into a certain direction (Figure 9, b). The second step of the processing workflow consisted in tiling the LiDAR files into 60*60 m tiles with a 5 m buffer. The 5 m buffer is necessary in order to prevent artefacts at the edge of the tiles. The size of the tiles optimized for the most efficient core usage. The third step was done with LASnoise to filter out isolated artefacts from the point cloud that can be created from a variety of factors such as birds and insects (Figure 9, c).

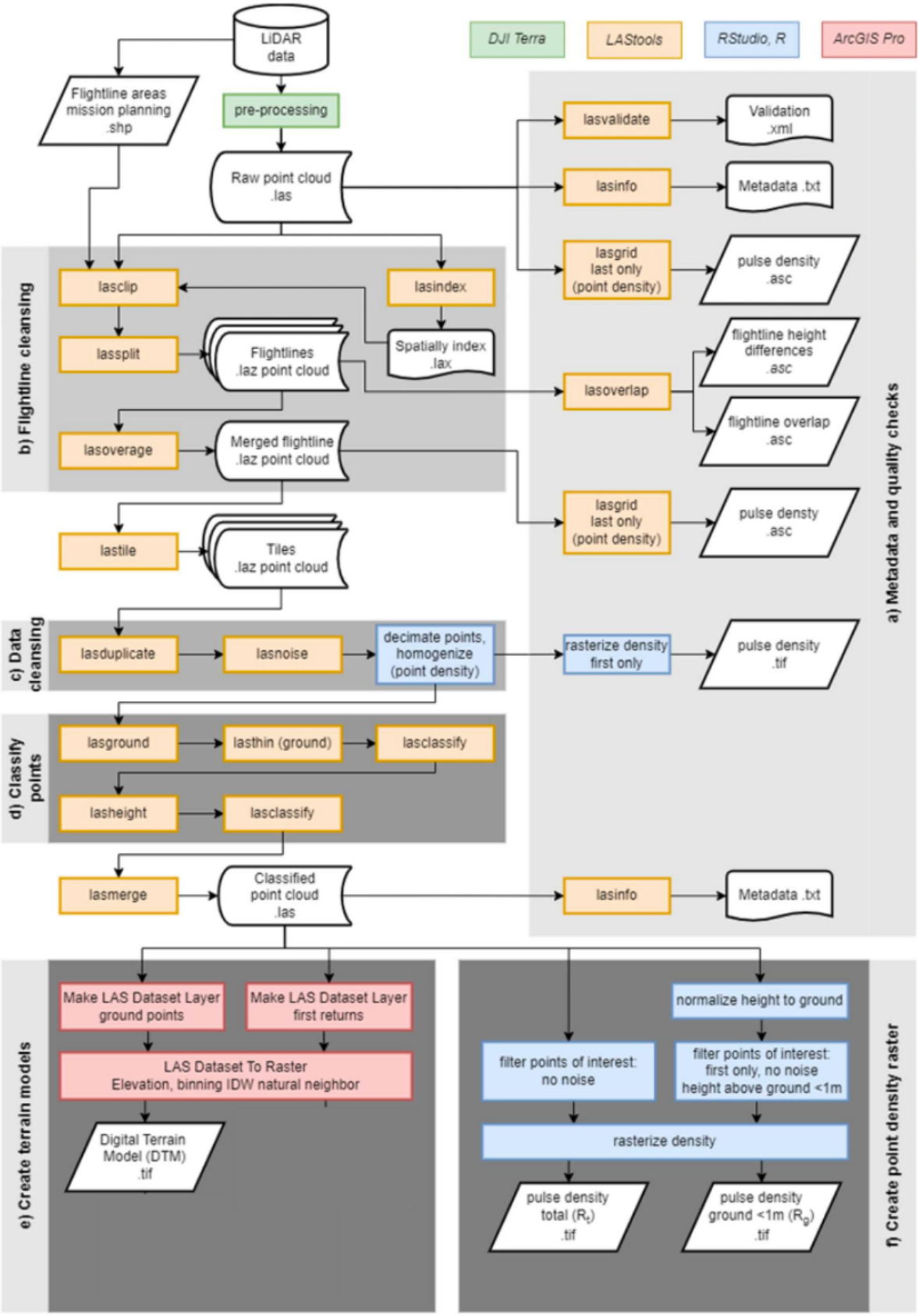

Figure 9 Layout of the LiDAR workflow (Hegels, 2023)

The fourth step, the ground classification was conducted with LASground (as visible in Figure 9, d). This step is crucial to achieving accurate end products. Yet, it proves difficult to conduct as the ground classification has to work in a variety of environments from dry upland areas to wetland. Therefore, 5 seismic lines were chosen with different ecosite types, line widths and management status. Then the following parameters: *Step*, *Offset*, *Bulge* and *Spike* were optimised to work well in all environments. The results of the classification were visualised using Fugro Viewer software (see Figures 10 and 11) in order to observe how vegetation and ground were separated. The result of this classification was a thick ground layer that includes the low ground vegetation such as *Labrador Tea.*

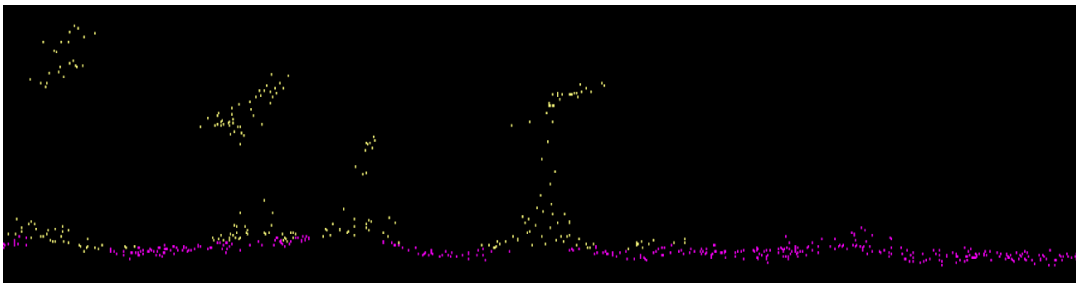

Figure 10 Ground classified points in pink, notable gaps visible.

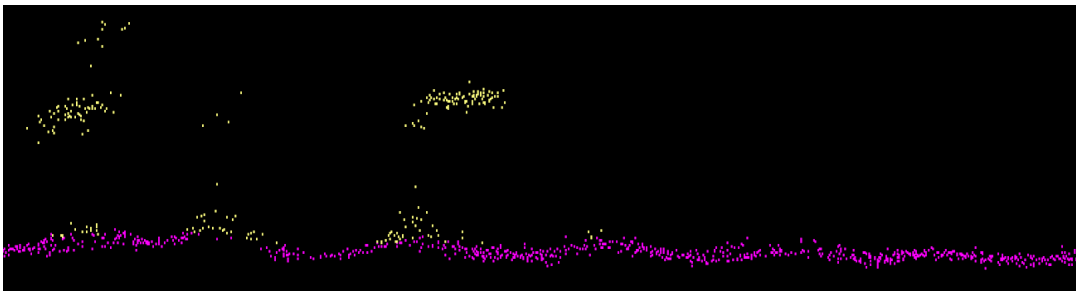

Figure 11 Corrected classification, with continuous ground points.

In the fifth step LASthin was used to filter out the upper points, only the lowest points were kept, in order to filter out the shrubby vegetation. In the sixth step the R package LiDR was used to filter the point cloud to a uniform 147 points per m^2. This was done to eliminate artefacts that come from a variety of factors such as the drone hovering to calibrate its IMU sensor.

In order to transform the ground classified points into the DTM, ArcGISpro was used, as it offers a diverse range of settings for terrain model creation (Figure 9, e). The interpolation type used, was the nearest neighbour binning method to create rasters with a pixel resolution of 15 cm for the high resolution LiDAR dataset. Therefore, every pixel is derived from 3 - 5 points.

3.4.1 Validation and statistical Analysis of LiDAR Workflow

The accuracy of the RPAS LiDAR and the plane based LiDAR datasets was measured by comparing the Z-values between the generated DTM and the RTK measurements. This was done via the RASTER package in R (Appendix). The statistical metrics to analyse the results were selected based on the work of previous studies conducted in this field (Harwin & Lucieer, 2012;, Lovitt, 2017). These include the root mean square error, mean error, median error. To determine if the differences between the classes and datasets are significant, a two-way mixed model ANOVA test ($\alpha = 0.05$) and a Tamhane's pairwise comparison was performed in R.

3.5 Quantification of Microtopography

In order to assess the state of the microtopography on seismic lines it is necessary to find metrics that quantify the state of microtopography. In this thesis three different ways of quantifying microtopography are used, all based on the high resolution DTMs generated out of the RPAS LiDAR point cloud. Figure 12 below shows the workflows employed.

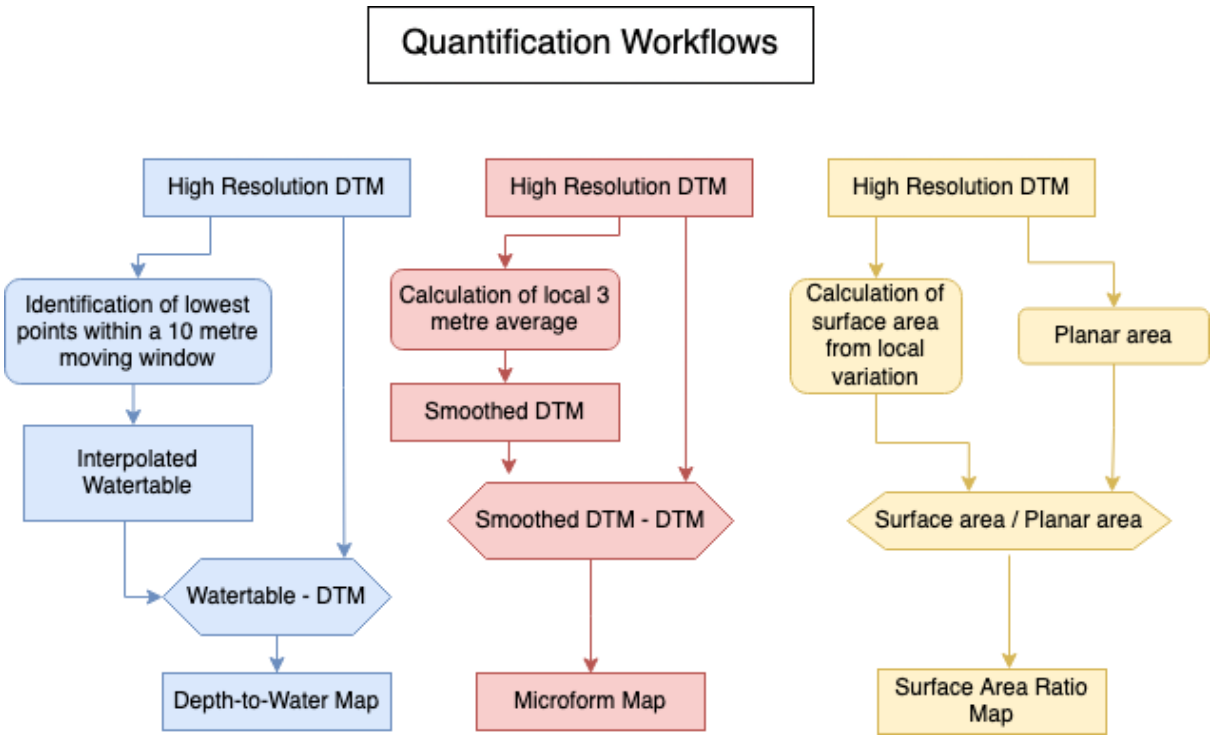

Figure 12 Layout of the quantification workflows.

3.5.1 Moving Window Classification

The microform workflow used in this thesis, is based on the workflow employed by Lovitt, 2017 to measure microtopography using a moving window as illustrated by Figure 13 reference surface was created by averaging each value of a high-resolution DTM with the surrounding three metres. This resulted in a smoothed surface, which was then subtracted from the high-resolution DTM. The outcome was a map with both positive and negative values. In this map, values above zero are considered as hummocks, while values below zero, represent hollows. The workflow was implemented using the focal function of the Raster package in R.

3.5.1.1 Validation of Moving Window Classification

To evaluate the accuracy of this workflow, the random point cluster dataset collected in the poor fen was employed. For every cluster the difference between the lowest and the highest points was calculated. This resulted in a dataset of in-situ range measurements. To extract the range measurements from the microform map, the values from the highest and lowest values were extracted, and the range between them calculated. These values were then compared. This workflow was conducted using the sp, deplyr and raster packages in R.

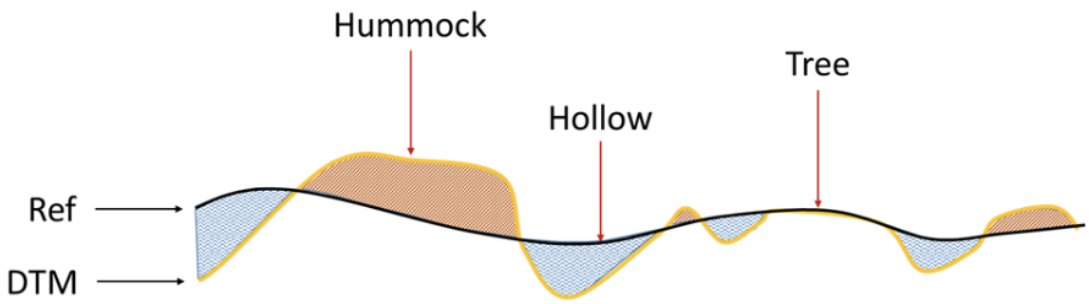

Figure 13 The classification of microforms via the reference DTM, created from 3 m moving window.

3.5.2 Surface Roughness

This study will attempt to use ruggedness in order to characterize the microtopography characteristics. Surface roughness can be calculated from a number of ways. The terrain ruggedness index (TRI) developed by Riley et al., 1999, has been used frequently by researchers to quantify surface roughness. It uses the matrix of the surrounding elevation values, usually a three by three grid and then calculates the square root for these. However, this method is difficult to compare to in-situ field measurements. One method that is easy to compare to in-situ methods is the surface area ratio (SAR) developed by Jenness, 2004. The SAR calculates

the surface area and divides it by the planar area. This results in minimum values of 1.0 for perfectly flat surfaces and higher values for irregular surfaces. The SAR was calculated using the Whitebox tools package available for R, that offers a wide range of geomorphometric tools to analyse point clouds and digital surface models (Lindsay, 2016).

One reason to apply the ruggedness index to measure microtopography is its potential in fractal analysis. We will therefore try to evaluate roughness at different scales to see if it is possible to use lower resolution airborne LiDAR available at a resolution of 30 points per m^2 to characterise the health of the hummock and hollow landscape.

3.5.2.1 Validation of Surface Area Ratio

To validate the surface area index, a script was written to calculate the surface length vs. planar length from the central transects as described in chapter 3.3.3. The code calculates the total length of the line by employing the Pythagorean theorem in three-dimensional space. It first computes the height differences and horizontal distances between consecutive points in each subset. Then, for each pair of adjacent points, it calculates the line distance as the square root of the sum of squared horizontal distances and squared height differences. Finally, all of the distances are summed up to obtain the total length of the line for each transect. This length is then divided by the planar length obtained by summing up the combined length of all the horizontal distances. The resulting value is then compared to the SAR value of the raster. This is done by extracting all x and y coordinates of the points making up the central transect and then averaging them to one value.

3.5.3 Depth-to-Water

To determine the DTW in peatlands, the methods in this work are leaning on the method created by Rahman, 2017, outlined in chapter 2.3.2.2. In contrast to the photogrammetric point cloud used by Rahman, the method described in this work relies solely on the high resolution LiDAR measurements. LiDAR technology, despite its numerous advantages, encounters significant challenges when applied to the measurement of the water table in peatlands. Firstly, LiDAR is not able to collect spectral information on the surface properties, therefore making it challenging to classify open water areas. Another one being that unlike photogrammetry, which can extract height information for points beneath the water surface, the LiDAR wavelengths most commonly used around 900 to 1000 nm are absorbed by the water surface. Therefore, there is no signal received from water surfaces.

The method proposed by this work aims to capitalise on the absorption of LiDAR by water surfaces. This method assumes that the lowest LiDAR point for a 10*10 metre square in a wetland area is very close to the water table, as there should be no LiDAR points beneath the water table. From the lowest point in each square a raster map is created for the entire wetland area, which is the assumed water table position. The water table raster is then subtracted from the high resolution DTM, to create a depth-to-water map for the wetland areas.

3.5.3.1 Validation DTW

To validate the accuracy of the water table measurements, the in-situ water table dataset collected in the poor fen was compared to the water table map generated as described in chapter 3.3.3. To validate the accuracy of the DTW workflow, the point cluster dataset from the fen was used to calculate an in-situ DTW. This was done by subtracting the water table measurements from the highest point measurement in the cluster. Then DTW for the highest point of the cluster is extracted from the DTW-map and the values are compared to the in-situ measurements.

3.6 Analysis of the Microtopography in the Kirby Fen

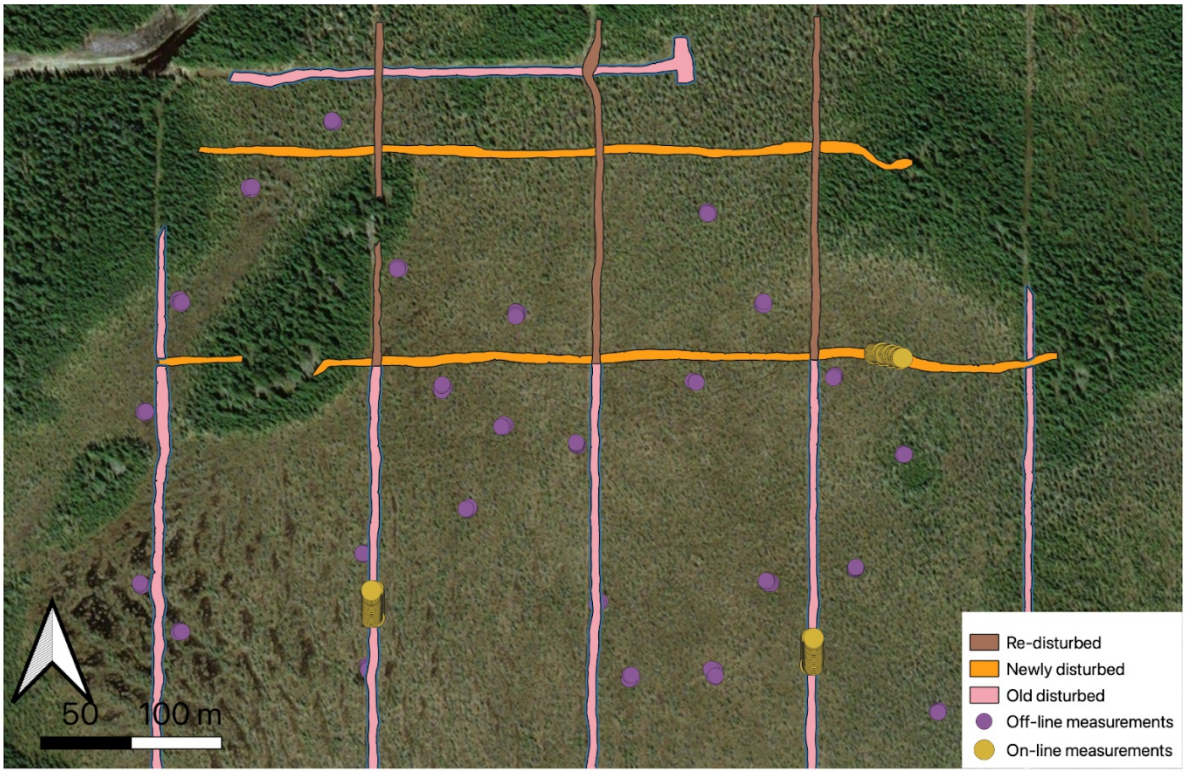

Figure 14 Study site in poor fen located in Kirby south. Active disturbance ongoing.

To analyse how the microtopography has changed on seismic lines, we will analyse the seismic lines using shapefiles of the seismic lines created by the forest line mapper. The undisturbed area was analysed with shapefiles located in the immediate surrounding area of the seismic line shapefiles. The seismic lines were differentiated between newly cut lines, re-disturbed lines and old lines, based on field visits (study area visible in Figure 14). We analysed the min, max and mean for the microforms measured by the moving window method and the SAR. For the Depth to Water this method is not suitable, since LiDAR cannot penetrate the surface of the water, therefore, only the max and mean height of the microtopography were analysed. Lovit, 2017 used some 30 shapefiles and averaged the measurements to give an overview how the minimum and maximum microform height is affected. This study will instead use the aggregate function of the Raster package in R, with a window size of 10*10 metres, which then produce an average maximum and minimum of the aggregate cells. To test if the difference between the disturbed areas and undisturbed areas is significant, the two tailed T-test (α=0.05) was conducted.

3.7 Aircraft LiDAR

A flight campaign to collect airborne LiDAR data was conducted by the company Airborne Imaging Inc. between June and August of 2022. The airplane flew at an attitude of 1800 metres above the ground and a speed of 160 knots. The LiDAR sensor employed was a Riegl VQ - 1560ii with a claimed accuracy of 20 mm horizontally and vertically. The claimed point density by the provider Airborne Imaging Inc. is 12 points per m^2. When measured in LAStools, the density is much higher at 30.75 points per m^2.

4 Results

The first section of the results will focus on the RPAS-LiDAR accuracy in fen areas, followed by a comparison with accuracy of an aircraft based LiDAR system. The second section will outline the accuracy of the different quantification workflows, while the third section will describe the application of the workflows, on a poor fen site.

4.1 Assessing the Accuracy of the RPAS LiDAR

The elevation accuracy assessment revealed significant differences in variances and mean accuracy among the various land cover classes (ANOVA test: $F = 320$, $p = 2.2e-16$).

The median elevation values varied across different land cover classes, ranging from -16 cm in UL 2 to 23.5 cm in UD 3. Notably, classes such as WT 1 and UD 4 exhibited a median elevation difference of less than 6 cm, indicating higher accuracy. However, for the entire dataset, the median elevation was found to be 7.4 cm, suggesting a tendency for the LiDAR measurements to overestimate the ground surface.

An analysis of the divergence between mean and median difference revealed a deviation greater than 1.5 cm in WT 3, WT 1, UL 2, UL 1, and UD 3, indicating a stronger influence of outliers in these classes. The RMSE for the entire dataset was calculated to be 20 cm, with UD 4 demonstrating the lowest RMSE of 9 cm, while UD 3 exhibited the highest RMSE of 30 cm. Tamhane pairwise comparisons were conducted to further investigate the elevation accuracy differences among the classes. UL1, WT1, and WT4 emerged as classes displaying the most significant differences compared to the other classes.

Table 1 provide a summary of the elevation accuracy assessment results, offering insights into the median, mean and RMSE observed among the land cover classes.

4.1.1 Differences between the Ecosites

The RMSE is 18 and 17 cm for wetlands and dry uplands, but is substantially higher for mesic upland sites at 23 cm (as visible in Figure 15). The median varies considerably throughout the ecosites, as upland dry tends to underestimate the ground surface by -6 cm, while the workflow substantially overestimates the ground surface in mesic uplands by 16 cm and 12 cm in wetlands. Higher variation of mean and median are found in upland sites, suggesting that these ecosites are more affected by outliers.

Metric	UD 1	UD 2	UD 3	UD 4	UL 1	UL 2	UL 3	UL 4	WT 1	WT 2	WT 3	WT 4
RPAS RMSE (cm)	18.8	24.5	30.2	9.0	20.8	19.5	13.4	15.2	19.7	12.2	20.1	17.7
RPAS Mean (cm)	14.4	20.3	25.7	6.5	14.0	-14.5	-10.0	-12.8	5.7	9.8	16.1	16.2
RPAS Median (cm)	13.2	21.4	23.5	5.3	12.5	-16.1	-10.1	-11.6	3.9	9.1	13.6	16.4
Aircraft RMSE (cm)	9.8	18.0	11.3	11.3	9.3	6.9	13.9	11.9	12.9	9.6	10.0	10.9
Aircraft Mean (cm)	-3.7	12.9	9.4	5.6	8.3	-9.0	-12.2	-8.4	-1.4	4.5	4.8	9.3
Aircraft Median (cm)	-3.9	14.5	9.9	5.5	8.1	-9.2	-12.3	-8.5	-1.5	4.6	4.9	9.4

Table 1 Accuracy of RPAS and aircraft LiDAR throughout the strata.

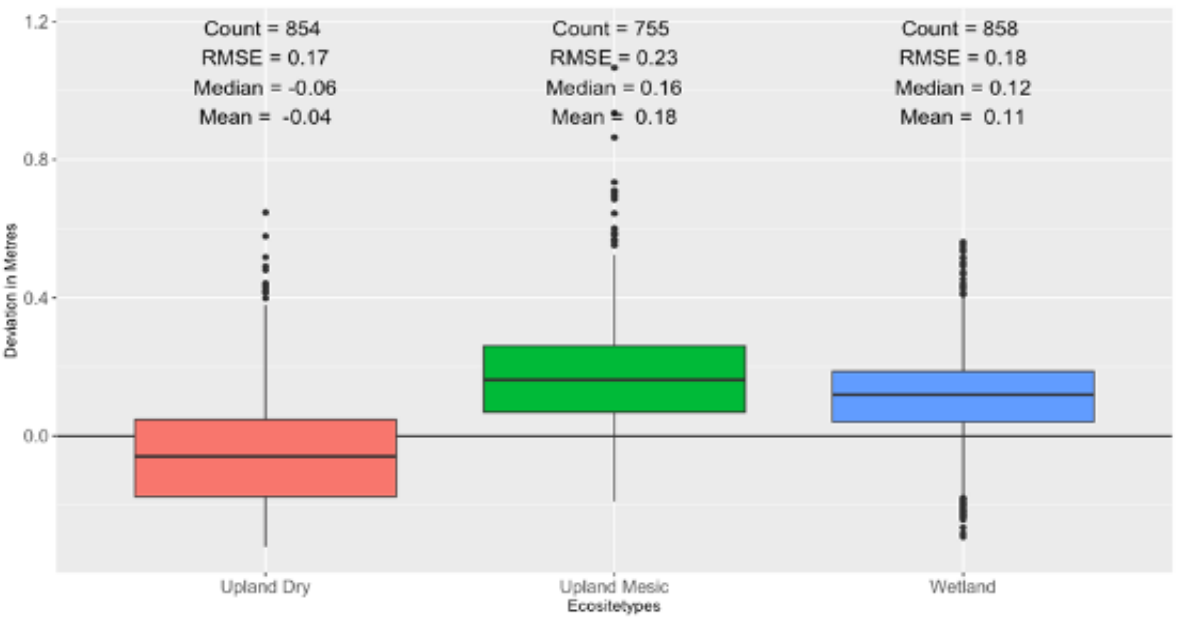

Figure 15 Performance of RPAS LiDAR throughout the ecosites.

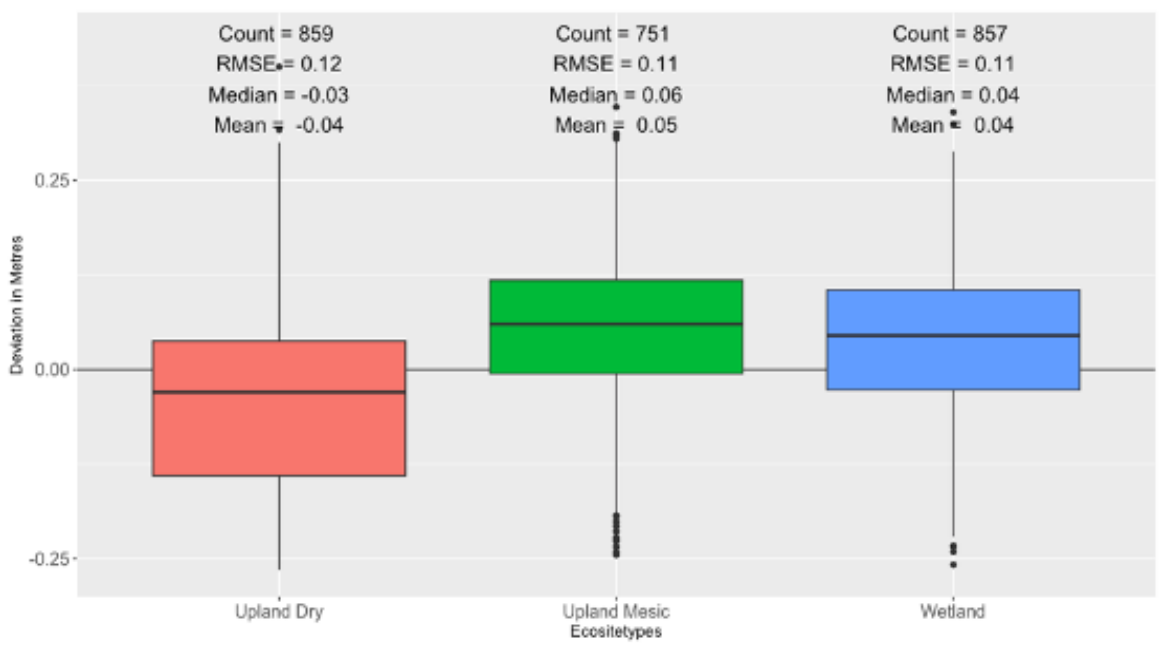

Figure 16 Performance of aircraft LiDAR throughout the ecosites.

4.1.2 Difference between the Seismic Line Types

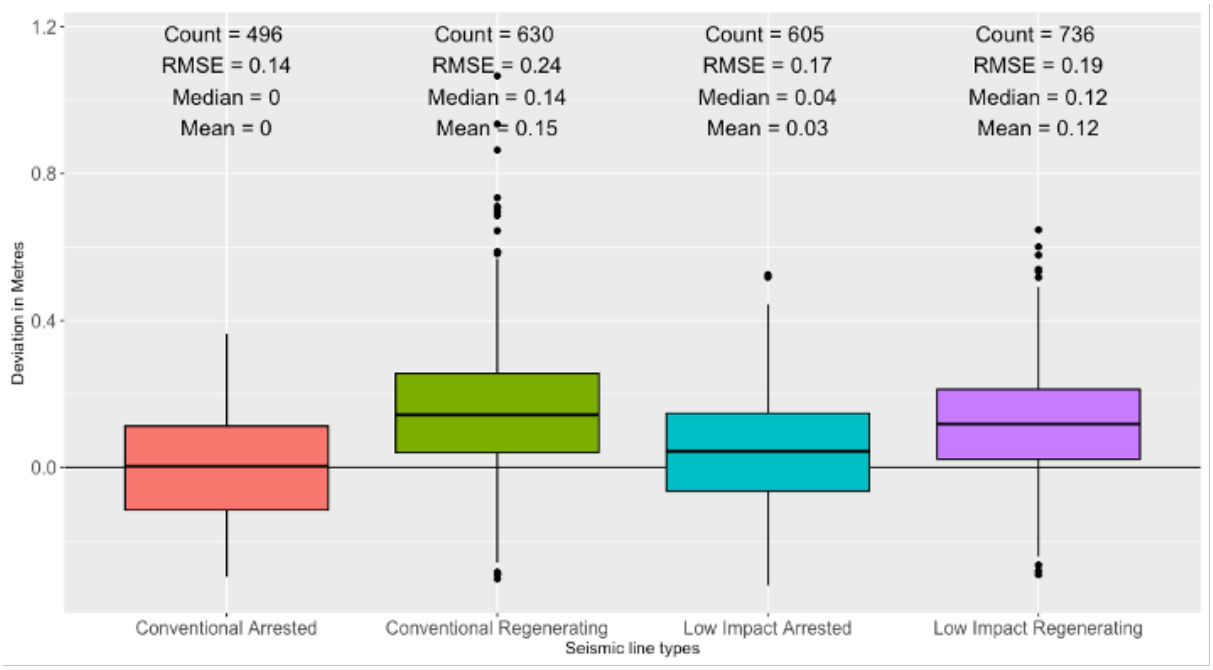

Figure 17 RPAS LiDAR Performance of different line types.

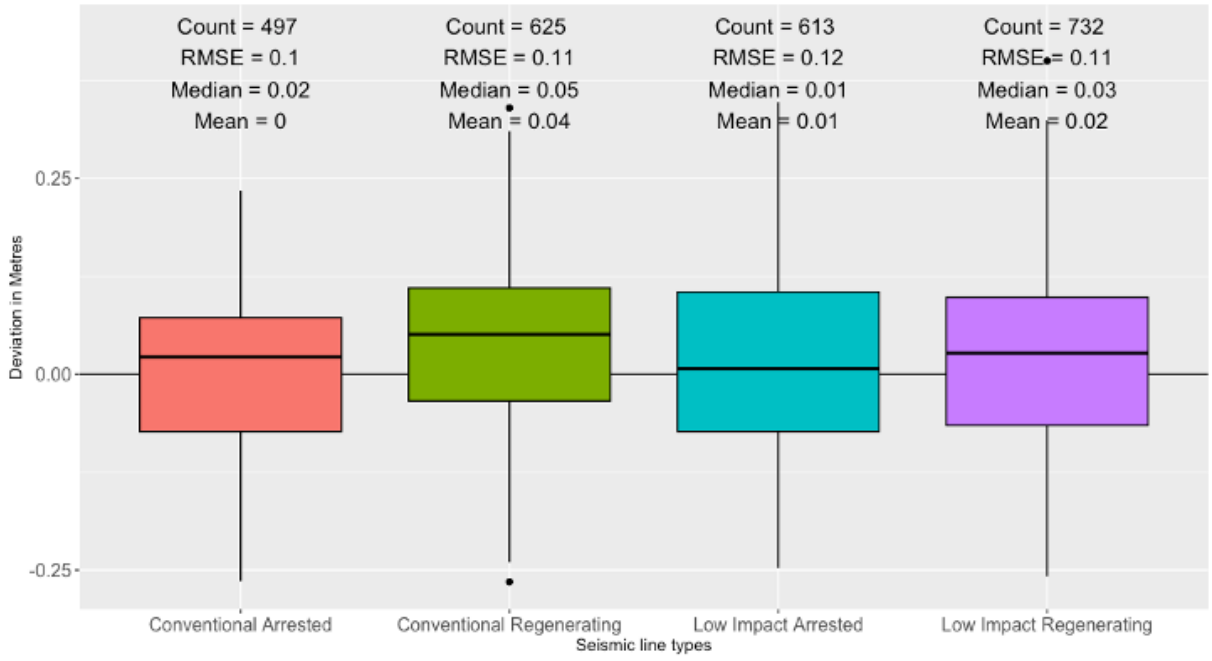

Figure 18 Aircraft LiDAR performance through different line types.

The difference between seismic lines in a state of arrested succession and regenerating lines is considerable, as visible in Figure 17. Lines in a state of arrested succession have a RMSE of only 8 cm, while lines in state of active regeneration have an RMSE of 17 cm. On lines in a state of arrested succession the median is 0 cm, while it is 9 cm for regenerating lines. The LiDAR quality on regenerating lines is also subject to more outliers, which push down the mean to 11 cm. When differentiating between line types, the RMSE is lowest on conventional lines in a state of arrested succession with 14 cm and slightly higher on "low impact" seismic lines in a state of arrested succession with 17 cm. On regenerating lines the RMSE is higher on conventional lines with 24 cm than on low impact lines with 19 cm. For all seismic line types the LiDAR derived DTM is overestimating the ground surface height with the median being 0 cm for conventional and 4 cm for "low impact" seismic lines stuck in a state of arrested succession. For regenerating lines the median drops to 14 cm for conventional and 12 cm for "low impact" line. The state of the vegetation seismic lines, has a significant influence (F = 315, p = 2e-16) on the accuracy of the LiDAR measurements (Figure 19 A and B)

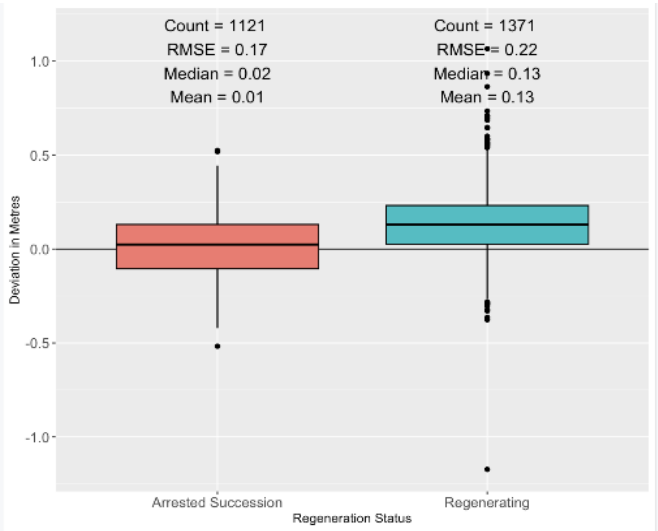

Figure A

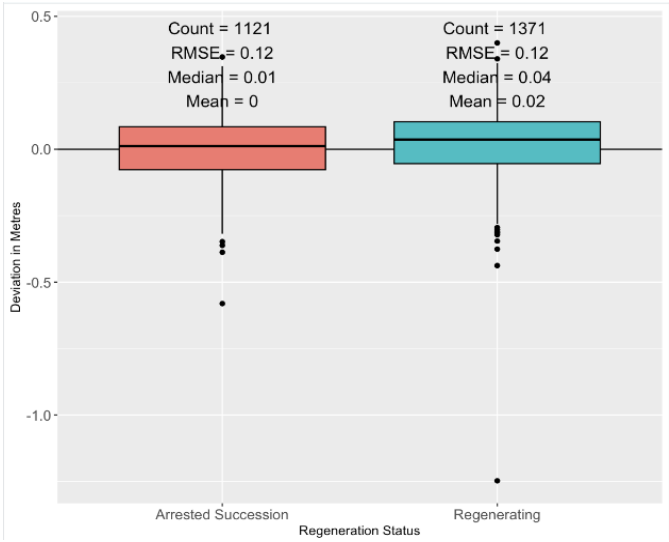

Figure B

Figure 19 ***A****: RPAS LiDAR performance between lines in arrested succession and regeneration.*
B*: Aircraft LiDAR performance between lines in arrest and regeneration.*

4.1.3 LiDAR Accuracy off Seismic Lines in a Wetland Area

The accuracy of the workflow suffers outside of seismic lines in peatland areas, as the RMSE drops to 19 cm compared to 11 cm for the measurements on the seismic lines in the same fen (as visible in Figure 20A). The overestimation of the ground surface is also more pronounced outside of the seismic lines with a median of 10 cm compared to 7 cm for seismic line surfaces. The increased ground complexity and higher vegetation cover found in areas adjacent to the seismic lines, therefore seems to be detrimental to the LiDAR performance.

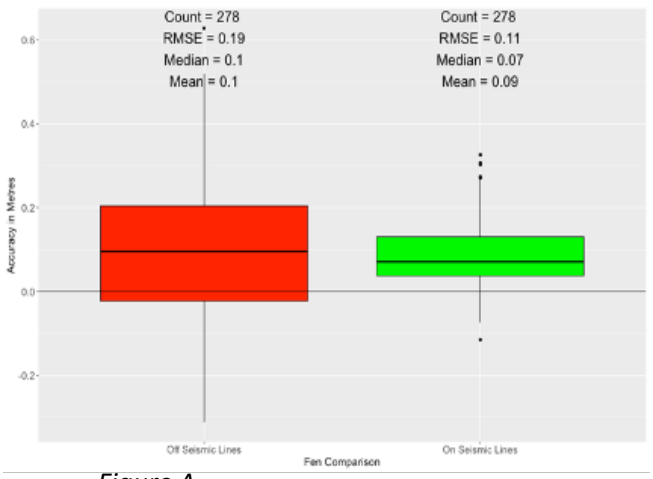

Figure A

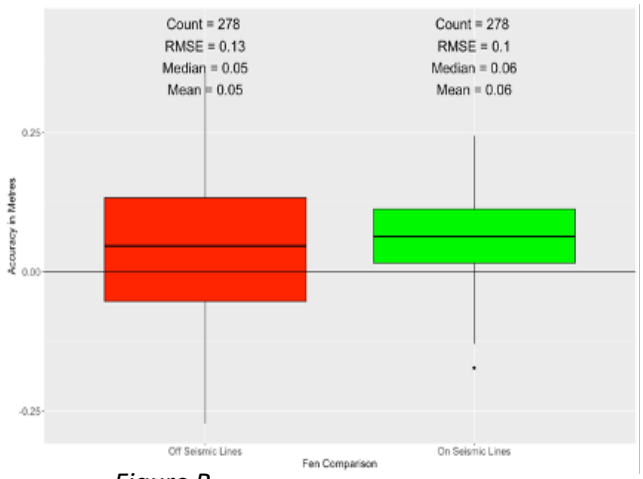

Figure B

Figure 20 ***A****: RPAS LiDAR performance off seismic lines and on seismic lines.* ***B****: Aircraft LiDAR performance off seismic lines and on seismic lines.*

4.1.4 Comparison to Aircraft LiDAR

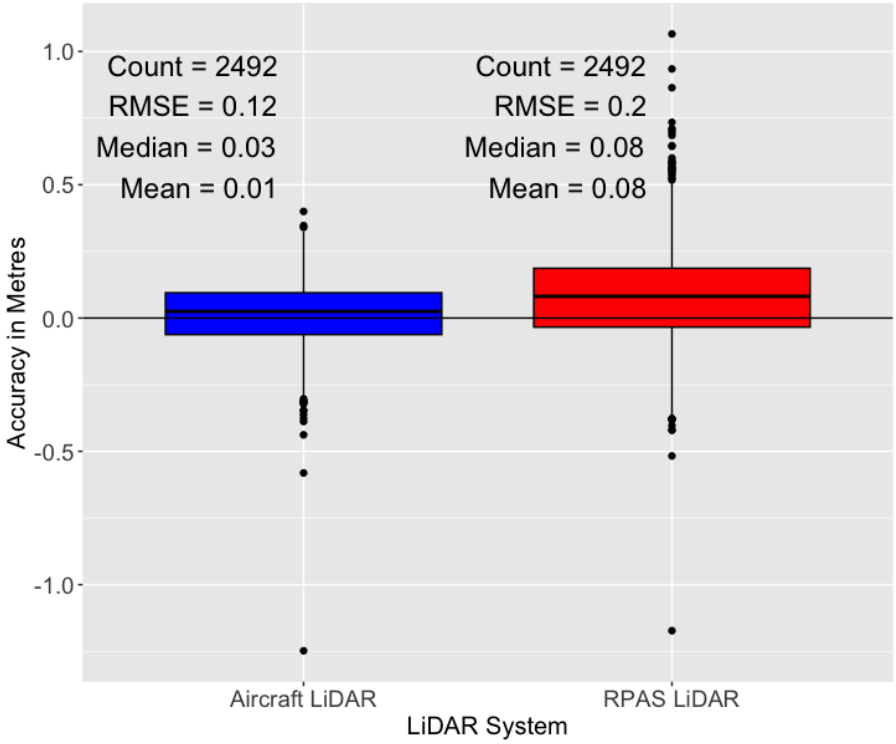

Figure 21 Comparison between aircraft LiDAR and RPAS LiDAR.

Airborne LiDAR outperforms the RPAS LiDAR as can be observed in table 1 and Figure 21. This is the case for all classes, except for UD 4, where the RMSE is 9 cm for the RPAS LiDAR and 11 cm for aircraft LiDAR. As visible in Figure 16, the aircraft LiDAR is less prone to outliers, suggesting a smoother surface generation. While both aircraft and RPAS LiDAR underestimate the ground surface in Dry Upland sites, the median is slightly higher for the

aircraft LiDAR at 3 cm compared to 5 cm for RPAS LiDAR. Both RPAS and aircraft LiDAR overestimate the terrain in Wetlands and Upland Mesic sites, but the overestimation is more pronounced for the RPAS LIDAR.

The aircraft LiDAR does not show great variation in the accuracy between lines in state of arrested succession and regenerating lines, as both classes have an RMSE of 12 cm as visible in Figure 18. The median of 4 cm points towards a slight overestimation of the ground surface on regenerating lines as it is only 1 cm on lines in a state of arrested succession. This compares very favourably to the RPAS LiDAR performance with a RMSE of 22 cm and a median of 13 cm.

When differentiating between conventional and "low impact" lines it becomes apparent that the accuracy is better on conventional seismic lines as the RMSE is 11 cm vs. the 13 cm on "low impact" lines. This is similar to the performance of the RPAS LiDAR, where the best RMSE is also achieved on conventional lines in a state of arrested succession. But RPAS LiDAR performs much worse on the conventional regenerating lines.

When comparing the performance of the aircraft LiDAR to the RPAS LiDAR off seismic lines in a wetland environment, the former is again performing worse. As the RMSE for the aircraft is only 13 cm vs. the 19 of the RPAS. Median offset is 5 cm for the aircraft LiDAR vs 10 cm for RPAS, suggesting that overestimation is less of a problem. Interestingly, offset is higher on seismic lines with 6 cm vs. 5 cm off seismic lines for the aircraft data, compared to 10 cm off seismic lines vs. 7 cm on seismic lines for the RPAS LiDAR.

4.2 Performance of Quantification Workflows

4.2.1 Surface Area Ratio

The Surface Area Ratio as derived from the LiDAR generated DTM is on average larger 1.052 SAR than the in-situ measurements with a value of 1.028 SAR (as visible in Table 2). Between the measurements there is large variation, this is especially pronounced for the regenerated wetland sites on conventional lines. Regenerated conventional lines seem to be prone to overestimation as visible in Figure 22, resulting in a r^2 of 0.03. The overestimation is much less pronounced on seismic lines in a state of arrested succession as visible in Figure 22, with an r^2 of 0.6.

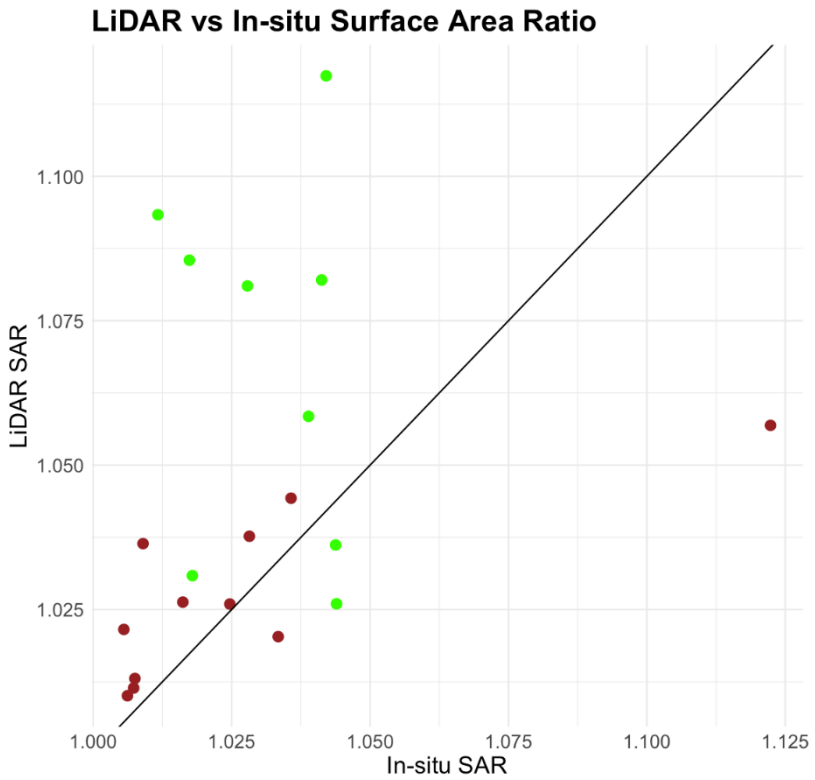

Figure 22 Performance of SAR in-situ vs LiDAR measurements.

Category	LiDAR	In situ	Difference
UL 1	1.06	1.043	1.63%
UL 2	1.041	1.074	-3.07%
UL 3	1.093	1.012	8.01%
UL 4	1.025	1.008	1.68%
ULD 1	1.058	1.028	2.92%
ULD 2	1.029	1.031	-0.19%
ULD 3	1.081	1.028	5.16%
ULD 4	1.016	1.006	0.99%
WT 1	1.042	1.041	0.1%
WT 2	1.035	1.026	0.88%
WT 3	1.156	1.034	11.8 %
WT 4	1.011	1.007	0.4 %

Table 2 Performance of SAR in-situ vs. LiDAR measurements.

4.2.2 Moving Window

The moving window method was assessed using the methodology outlined in chapter 3.5.1, the goal was to compare the variance between the lowest hollows and the highest hummock within a cluster. This resulted in 39 samples. This approach achieved a RMSE of 13.7 cm. The median of 8.2 cm and mean of 11 cm suggests that the range between the high and low points is slightly overestimated by this method.

4.2.3 Depth-to-Water Table

To assess the distance to water, first the accuracy of the LiDAR derived water table measurements is validated through the 105 in-situ measurements of the water-table, more on this in chapter 3.5.3.1 This resulted in an RMSE of 6.5 cm, a mean of 4.4 cm and a median of 5.1 cm. The correlation visible in Figure 23 between the measurements is very high.

The depth to water measurements are validated using the methods outlined in chapter 3.5.3.1, which calculated the distance to water by subtracting the level of the water table with cluster measurements, this was done for 39 samples. This resulted in an RMSE of 12.7 cm, a median of 7 cm and a mean of 5 cm. Suggesting that the overestimation of the ground surface by the LiDAR leads to an overestimation of the DTM.

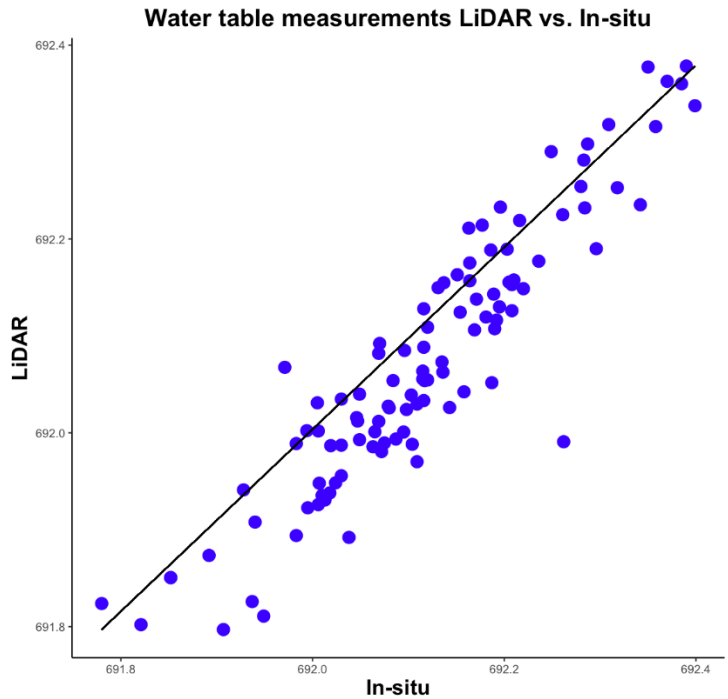

Figure 23 In-situ vs. LiDAR water table measurements.

4.3 Case Study: Kirby Fen

4.3.1 Impact of Seismic Lines on Microtopography

The analysis of the depth-to-water showed significant differences ($p = 0.01$) between the mean of disturbed and undisturbed areas. In the disturbed area, depth values fluctuate within a range of 5.838 cm at the minimum and 61.11 cm at the maximum, with an average depth measurement of 23.52 cm. In contrast, the undisturbed areas show depth values spanning from a lower limit of 5.3 cm to an upper limit of 63.13 cm. The mean distance to the water table in these areas is higher at 26.44 cm. All results are shown in Table 3.

The moving window methods also revealed significant ($p = 0.01$) differences between the mean values between the areas. In the disturbed areas, the range was distributed from -13.71 to 15.55 cm, with a mean value of -0.5 cm. Meanwhile, in the undisturbed areas, the range extended from -11.68 cm to 17.13 cm, with a slightly positive average of 5.12 cm.

Significant differences ($p = 0.1$) were also observed for the Surface Area Ratio. This method showed that in disturbed areas, SAR values varied from 1.006 to 1.57, with an average of 1.09. For undisturbed areas, the SAR exhibited a broader range from 1.01 to 4.11, accompanied by a marginally higher mean of 1.119.

The hummock/hollow ratio in disturbed areas was found to be 41/59, while in undisturbed areas it was slightly different at 43/57.

Metric	Disturbed	Undisturbed
Depth-to-Water		
Maximum	61.11	63.13
Mean	23.52	26.44
Moving Window		
Minimum	-13.71	-11.68
Maximum	15.55	17.13
Range	29.26	28.81
Mean	-0.5	5.12
Hummock/Hollow Ratio	43/57	41/59
Surface Area Ratio		
Minimum	1.006	1.01
Maximum	1.573	4.11
Range	0.567	3.1
Mean	1.109	1.119

Table 3 Disturbed vs. undisturbed areas for the different quantification methods.

4.3.2 Differences between Disturbances

Metric	New Disturbance	Old Disturbance	Re-Disturbance
Depth-to-Water			
Maximum	0.598	0.652	0.594
Mean	0.253	0.253	0.21
Moving Window			
Minimum	-0.134	-0.189	-0.123
Maximum	0.204	0.19	0.263
Range	0.338	0.38	0.387
Mean	0.002	-0.005	-0.013
Surface Area Ratio			
Minimum	1.014	1.017	1.022
Maximum	1.866	1.729	1.511
Range	0.851	0.712	0.489
Mean	1.13	1.122	1.11

Table 4 Impact of different types of disturbances quantified.

When applying the depth to water method significant differences between all three line types become apparent ($p = 0.01$). When comparing microform maximum height, old disturbances were measured with having the highest value of 65 cm followed by re-disturbances 59 cm and new disturbances 59 cm (as shown in Table 4. Interestingly, the mean values for new and old disturbances are identical at 25 cm, while re-disturbances have a slightly lower mean value of 21 cm.

When using the moving window methods, minimum values measured were lowest in old disturbances with 19 cm and around 13 cm for new and re-disturbances. The maximum values for new and re-disturbances are 0.204 cm and 0.263 cm, respectively, while for old disturbances, it is 0.19 cm. The largest range of 38.7 cm is seen in re-disturbances, closely followed by 38 cm in old, while new-disturbances are observed to have a lower range of 34 cm, indicating a higher variation in re-disturbances and new-disturbances. The mean values for all types are very close to zero.

New disturbances have both the highest maximum value (1.866) and the largest range (0.851). On the contrary, re-disturbances have the smallest maximum value and range, indicating that these disturbances tend to affect a smaller area compared to new and old disturbances, and also show less variability. However, the mean values for all types of disturbances are fairly close (between 1.11 and 1.13), suggesting that, on average, the area affected by different types of disturbances is relatively similar.

5 Discussion

5.1 Performance of RPAS LiDAR Dataset

The analysis of the accuracy of the LiDAR dataset reveals a great variance between the sites. The high variance is not always correlated with the ecosite, seismic line type or regeneration status. This suggests that apart from the strata designed to capture the most important variables, more environmental factors have a substantial influence on the accuracy.

Firstly, slope seems to be a major factor in creating error in LiDAR measurements. The rapid terrain changes on sloped sites were found to quickly amplify terrain error, and therefore lead to less accurate measurements. Interestingly, on some slopes this results in overestimation of the ground surface, while on other slopes it leads to an underestimation of the ground surface.

For the majority of sites the RPAS LiDAR tends to overestimate the ground surface. While this might correspond to a higher gradient in some sites, it is very persistent throughout the wetland sites, with no substantial slope. This is likely explained by the shrubby vegetation found in these wetland sites, which has been noted by Moudrý et al., 2020 to block laser pulses from penetrating to the actual ground surface or confuse the ground classification. On the other hand, underestimation of the ground surface only occurred in Mesic Upland and Dry Upland, on sloped sites (more on slope in chapter 5.1.1).

5.1.1 Differences between the Ecosites

Substantial differences between the ecosites were notable. Especially Mesic Upland sites stood out, for their high RMSE of 23 cm and their high overestimation of the ground surface. Several factors may contribute to this low accuracy: Mesic uplands are often dominated by deciduous stands of aspen, which surround the seismic lines and limit the angles from which LiDAR can penetrate to the ground surface. Another being that even if the line is stuck in arrested succession, the surface vegetation of seismic lines is often complex and overgrown by broadleaved bushes further limiting laser pulses reaching the ground surface. Finally, the sloped nature of these sites combined with few points reaching the ground surface leads to large interpolation errors between points. This observation echoes findings by Bater and Coops, 2009 which highlighted similar problems in sloped terrain.

Dry upland sites are found to have a much better RMSE of 17 cm and a median of -6 cm, making it the best performing ecosite. While slope may still be a factor, the surrounding forest

stands are generally thinner, dominated by spruce and pine trees, and contain less deciduous trees, than the mesic uplands, which allows more laser pulses to reach the ground surface. The ground surface itself is defined by lichen and thin sedges such as *Carex siccata* and *Carex tonsa*. The low complexity of the vegetation covering the ground is likely another factor leading to the good results as it hardly confuses the ground classification or hinders laser penetration.

The wetland ecosites have an RMSE of 18 cm, which is only slightly worse than the Dry Upland sites. This is likely a consequence of the thinner tree cover, often consisting of coniferous trees such as tamarack and black spruce, which is easier to penetrate by laser pulses. Additionally, the sites display a complex surface structure consisting of sphagnum and feather mosses that are often covered by shrubby vegetation, which may hinder the effective penetration to the actual ground surface in peatlands. The occurrence of complex surface vegetation is a possible explanation for the overestimation of the ground surface by 10 cm. Another reason for the overestimation may be that the ground surface often consists of live plant matter, which is difficult to define and may thus confuse the ground classification of LiDAR pulses.

5.1.2 Differences between seismic lines

During the analysis a major factor determining the accuracy of the LiDAR on seismic lines was the regeneration status. A regenerated status decreased RMSE on conventional lines from 14 cm to 24 cm and from 17 cm to 19 cm on “low impact” lines. Regeneration also increased the median offset to 14 cm on conventional and 12 cm on “low impact” lines. One major driving factor of the lower accuracy is the high presence of outliers, that resulted from vegetation being mistaken for ground or causing interpolation error. While the presence of thick vegetation appears to be a major obstacle to achieving very accurate ground measurements, the higher error on regenerating conventional lines compared to "low impact" lines might be amplified by the fact that more of these sites were located on sloped terrain.

For lines in a state of arrested succession, conventional lines achieved the highest accuracy. The superior performance compared to “low impact” lines may be explained by the wider canopy opening, allowing the LiDAR to penetrate from more angles. The reduced ground complexity of the lines in a state of arrested succession, likely contributed to a generally low median offset of 0 cm on conventional and 4 cm on “low impact”.

5.1.3 LiDAR Accuracy on and off Seismic Lines

When comparing the accuracy of measurements on seismic lines in a wetland vs. the surrounding areas, it becomes apparent that measurements off seismic lines are less accurate than on seismic lines. One major factor driving the higher RMSE and offset might be the higher level of microtopography, creating small scale steep gradients that are more difficult to detect by the LiDAR. Additionally, the microforms often form the habitat for dense shrubby vegetation, making the differentiation of hummocks and shrubs complex. Another factor driving less accurate measurements off seismic lines is the higher tree cover lowering the point density on the ground.

5.1.4 Performance of RPAS LiDAR vs. Aircraft LiDAR

This study underscores the comparative advantage of airborne LiDAR vs. RPAS LiDAR in various settings. The observed underestimation of ground surfaces in Dry Upland sites by both LiDAR systems, highlights uniqueness of this terrain type, however the airborne LiDAR seems to handle the complexity of increased gradients much better. The fact that both LiDAR systems overestimate terrain in Wetlands and Upland Mesic sites, with a more pronounced overestimation by RPAS LiDAR, is noteworthy. The consistency of performance by airborne LiDAR across different states of succession and regenerating lines underscores its robustness and reliability. This finding aligns with the work of (Zolkos et al., 2013), who highlights the ability of airborne LiDAR to deliver reliable data across varying vegetation stages, which they attributed to the superior canopy penetration capability.

The substantially better performance of the aircraft LiDAR using a point density of only 30 points per m^2 compared to the RPAS LiDAR using a point density of 147 points per m^2 was unexpected and suggests that other factors than point density are important to the performance of LiDAR systems. One factor might be the Zenmuse L1 sensor that is constricted in size and weight in order to fit on RPAS vehicles, which limits the quality of the sensors electronics, lowering the accuracy of the laser measurements to 10 cm horizontally and 5 cm vertically. In contrast, the Riegl VQ-1560ii has the ability to perform full waveform analysis, meaning that it can detect very small return time differences, which according to the manufacturer allows for an accuracy of 2 cm horizontally and vertically.

A further variable might be the less stable platform provided by the RPAS system, flying in more turbulent lower atmospheric layers, which coupled with the less accurate IMU-unit might

lead to larger offsets between measurements. The GNSS RTK system of the DJI Matrice 300 also comes with a ground station that is difficult to adjust on the horizontal axis, especially under field conditions. This might also increase horizontal error.

Another factor that might contribute to the better performance of the aerial LiDAR accuracy, may be a superior workflow employed by the provider Airborne Imaging Inc.. Adjusting one workflow to a number of different ecosites is difficult, as has been shown by (Nelson et al., 2022). A better processing workflow might adjust parameters in different terrain types and correct for over and underestimation of the ground surface. This however is speculative, as no specifics on the processing workflow employed by Airborne Imaging Inc. were published.

5.1.5 Comparison to other Studies

The accuracy of the RPAS LiDAR is similar to the results achieved by Nelson et al. 2022. The multispectral LiDAR aircraft based measurements performed in similar environments located close to the study sites used for this study. Nelson et al.,2022, achieved an RMSE of 19 cm which is close to the 20 cm of our study.

The photogrammetry study performed by Lovitt et al. 2017 in wetland and upland areas achieved very similar results to our study with slightly worse results in low complexity wetland areas, somewhat comparable to our measurements on seismic lines in a state of arrested succession in wetland areas. In these areas this work achieved achieved an RMSE of 12.8 cm and a median offset of 9.1 cm compared to the 21 cm RSME and median offset of -10 cm of the photogrammetry. When it came to complex terrain roughly comparable to regrown seismic lines this study on average achieved an RMSE of 22 cm and a median offset of 13 cm, which compares very favourably to the 42 cm RMSE and 47 cm offset in Lovitt et al., 2017.

The superior performance of the LiDAR in the complex terrain encountered in the boreal landscape, might be explained by the higher point density of 147 p/m^2 that exceeds the point density of the older photogrammetry system of 84 points per m^2. Newer higher resolution photogrammetry sensors like the Zenmuse P1 sensor might be able to improve the accuracy but will likely struggle to match the performance of modern LiDAR systems, as the SfM feature matching algorithms struggle to reliably identify tie points in complex terrain (Mancini et al., 2013). Therefore, using RPAS based LiDAR or aircraft LiDAR is preferable in most contexts when trying to identify the ground surface in peatlands.

5.2 Performance of Methods to quantify Microtopography

5.2.1 Surface Area Index

The method of quantifying microtopography via the SAR was validated with mixed results. In general an overestimation of the surface area was observed. On the seismic lines in a state of arrested succession the relationship between in-situ and LiDAR measurements seems to hold much better. This suggests that this SAR should work reasonably well in quantifying microtopography on seismic lines that are in need of restoration work.

Overestimation was more pronounced on regenerating seismic lines, especially in wetlands. Classes that had a higher RMSE compared to the RTK measurements, such as UD 3, UL 1 and WT 3, tended to also overestimate the SAR to a larger degree. The denser surface complexity of the regenerated sites and the higher ground vegetation likely contributed to the exaggeration of microform height and lowered accuracy.

Other reasons for the mixed performance of SAR might be connected to the different ways microtopography was measured. While the LiDAR based SRI measured the difference to the surrounding cells in a matrix, the in-situ measurements measured the SAR in a line. This might introduce a bias in the measurements, as many seismic lines feature trails, or vehicle paths, which are often located adjacent to the central transect and create microtopography, which is only captured by the LiDAR derived SAR. However, the relatively low number of transects available to validate this method limits the validation of SAR. The transects to check the SAR were time consuming to measure, therefore ideally a quicker method of validating the accuracy of the SAR would be desirable for future studies investigating SAR.

5.2.2 Depth-to-Water

Following the workflow proposed by Rahman et al. 2017, the attempt to create a metric that is reflective of depth to water, yielded very good results in the peatland area it was implemented in. The RMSE for water table measurements of 6.5 cm outperforms the accuracy of the surface measurements in the fen area which had an RMSE of 19 cm. This suggests low points can be identified very accurately. The accuracy of the results are very close to the results Rahman et al. 2017, which achieved a RMSE of 10 cm in favourable terrain and a RMSE of 22 cm for the whole study area including upland areas.

The RMSE of 12.7 cm and the median offset of 5.1 cm for the DTW method compares unfavourably to the more accurate water table measurements. This is likely a consequence of the LiDAR performing poorly when measuring the fen surface (RMSE of 19 cm).

The basic assumption of the Rahman et. al. 2017 workflow relies on open water being equal or close to the water table. This in turn relies on open water being present and being detectable from spectral information from the photogrammetry data. Since the workflow of this study relies only on LiDAR measurements and cannot identify open water surfaces, it should only be applied in areas with a high certainty of open water being present. This limits the measurements of DTW metrics to wetlands with low gradients and a relatively high water table. The workflow performs poorly in measuring microtopography on slopes mainly due to the fact that it relies on a relatively large moving window of 7 meters to identify low points representative of the water table. Although the water table may still be measured correctly, the DTW is not a useful metric of microtopography in this context, as it will spike to large values, insensitive to microforms.

5.2.3 Moving Window

The moving window method using the average height of the surrounding three metre window performed well in measuring the average range between hummocks and hollows. For the study area in the fen, the RMSE was only 13.1 cm and the median 8.2 cm. It therefore appears to be reliable in detecting the variability of microforms in the fen. The moving window approach was however problematic in sloped environments, as the moving window will tend to over and underestimate the ground surface in these environments visible in Figure 25. While a smaller window size would be beneficial in sloped environments, it would also negatively affect the measurements on seismic lines. This negative effect arises due to the local bending of the moving window average, consequently diminishing the value of statistical metrics such as mean height.

The hummock and hollow classification scheme derived from this moving window approach, proved to be highly inaccurate, as it recorded an accuracy of less than 50 %. This might be a consequence of the layout of the verification dataset, as the original purpose of the dataset was to test the performance of the LiDAR and it therefore included many intermediate points between hummocks and hollows, that were difficult to classify. Better results might be achieved, if these points were placed more centrally on microforms, , which however would not test the horizontal accuracy of the system as well.

5.3 A Study of Microtopography in a Fen Area

5.3.1 Distance to Water Workflow

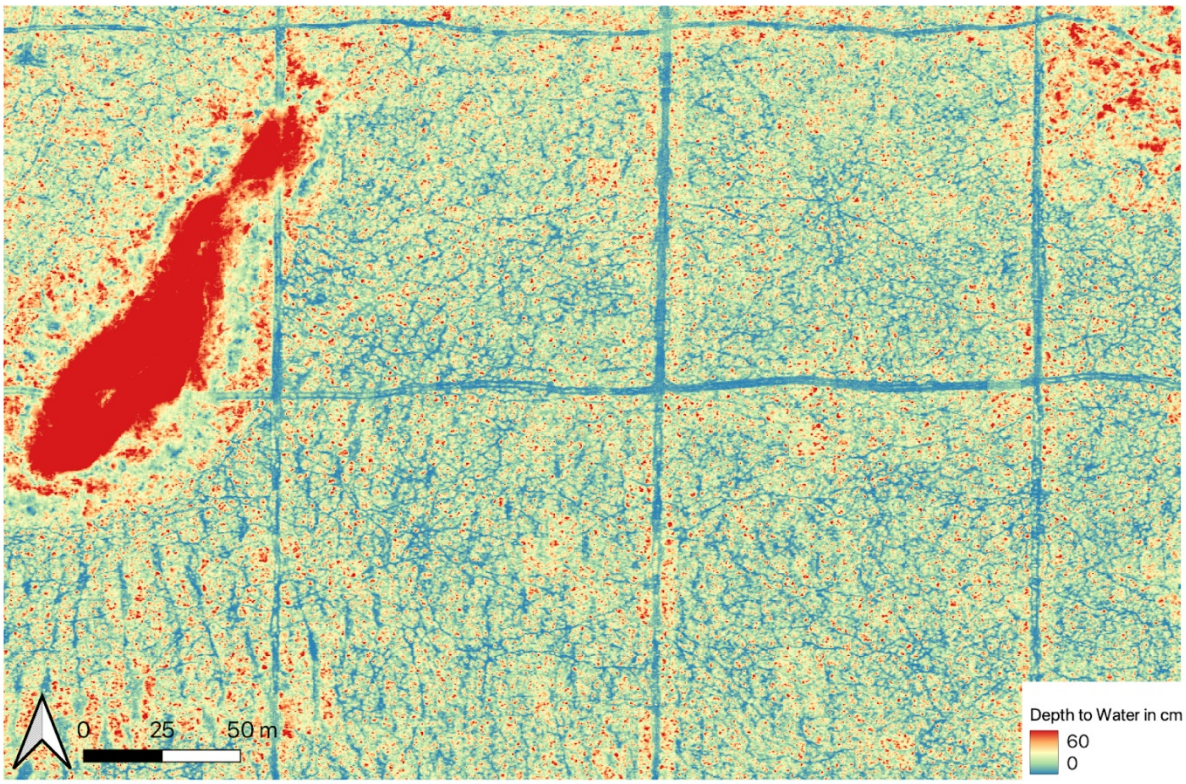

Figure 24 Distance to Water map shows that new disturbances are clearly visible, while older disturbances start to blend in with the surroundings. Saturation obscuring microtopography measurements occurs in upland areas.

The impact of the seismic activity on the microtopography in the wetland area was observed to be significant for the DTW method. When comparing disturbed and undisturbed areas, a slight reduction of hummock height by 2 cm, and a reduction of 3 cm for the mean depth-to-water values was observed in disturbed areas. This indicates a depression of seismic lines compared to the surroundings. However, the measured mean offset of the LiDAR-DTM on seismic lines was measured to be 9 cm vs 10 cm in undisturbed areas. Therefore, the actual difference between the mean DTW might be slightly lower than measured. Nevertheless, a considerable difference between the areas remains. The difference in maximum height measured between the areas is very close to the results of Lovitt et al. 2018, which were 24 cm in undisturbed areas and 21 cm in disturbed areas. Since the photogrammetry of Lovitt et. al. 2018, was able to penetrate beneath the water surface, the mean depth to water was negative for both areas, with disturbed areas being depressed by 15 cm, a significantly greater difference than the 3 cm this study measured. As visible in Figure 24 the DTW method, quickly loses its utility in measuring microtopography when exposed to gradients.

5.3.2 Moving Window Workflow

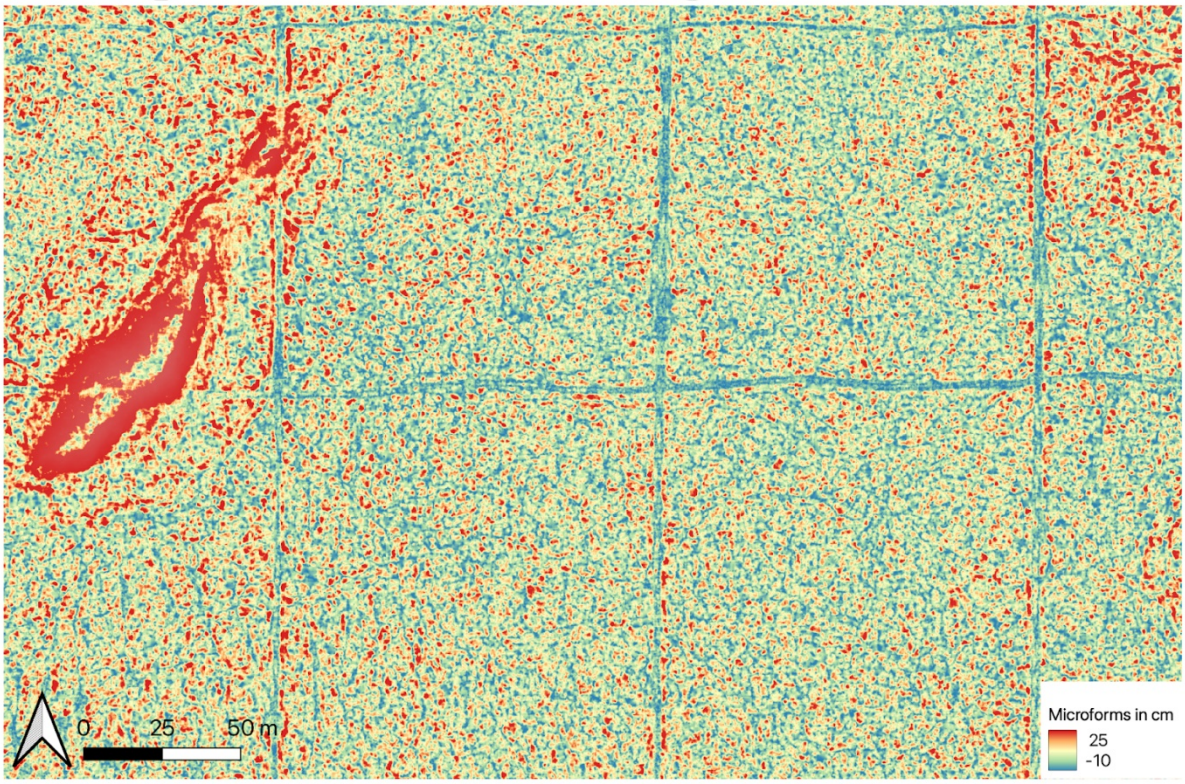

Figure 25 Map of moving window shows new disturbances clearly but struggles more than DTW to identify older lines.

The microform method also showed significant differences between the disturbed and undisturbed areas. The disturbed areas were shown to have on average 2 cm deeper hollows, and 1.5 cm lower hummocks. The range between disturbed and undisturbed areas was similar with only 5 mm difference. The biggest difference apparent in the data is the much lower mean height of -0.5 cm in disturbed areas vs. 5 cm in undisturbed areas. This suggests the microtopography is severely depressed in disturbed areas (as visible in Figure 25). The study of Lovitt et. al. 2018 recorded a much bigger range difference between disturbed and undisturbed areas, but the ability of the photogrammetry to look beneath the water surface likely contributed to this. The mean height differences between disturbed and undisturbed areas recorded by Lovitt et. al. 2018 were much smaller, this might be due to the smaller moving window size of 2 metres compared to the 3 metre window used by this study.

5.3.3 Surface Area Ratio Workflow

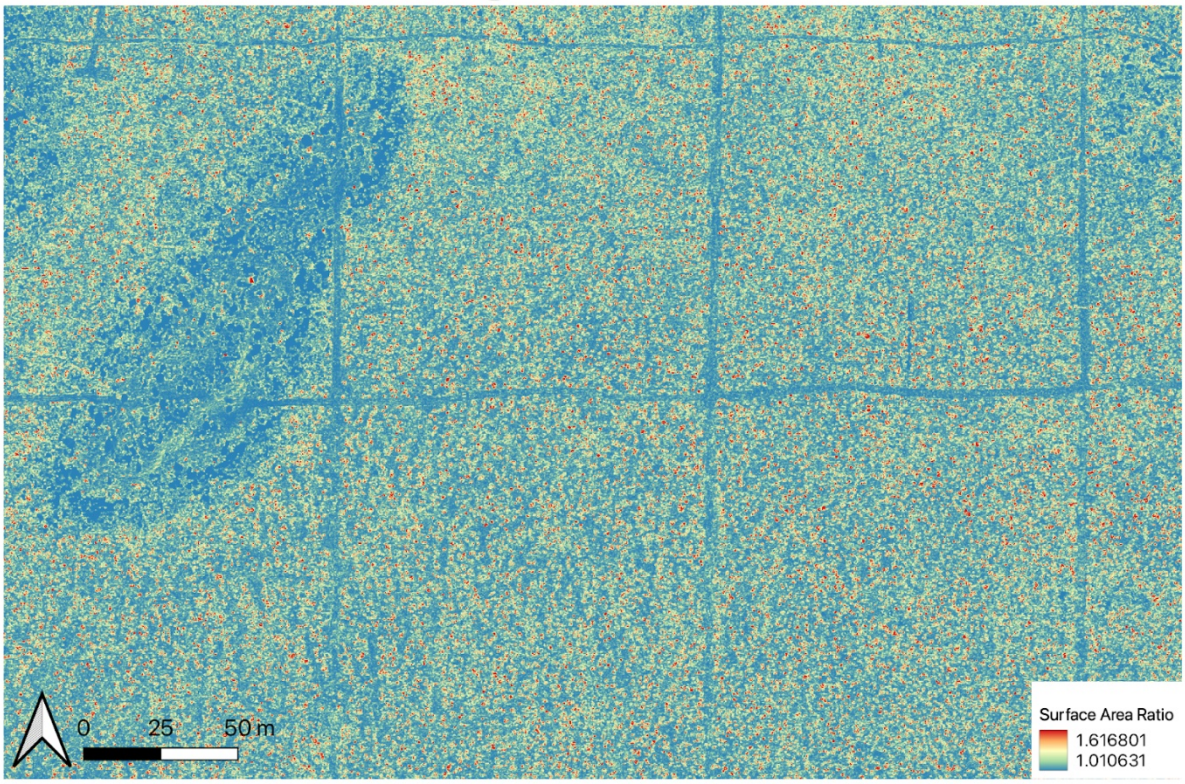

Figure 26 Surface Area Ratio map shows disturbances clearly even through the upland area.

When comparing the surface area between the disturbed and undisturbed areas in the fen (as visible in Figure 25), it becomes clear that there are significant differences in the maximum surface area. Undisturbed areas experienced significant spikes in surface area compared to the disturbed areas. It is unclear what causes these extreme spikes to up to 4.1 SAR, but they might be a result of faulty ground classification, which includes shrubs or trees, therefore dramatically increasing the local surface area. With a value of 1.86 the maximum surface area on seismic lines is dramatically lower at 1.86 SAR. Therefore, the maximum surface area seems to be an unreliable measure in detecting differences between disturbed and undisturbed areas. When comparing the mean a slightly lower value is measured for the disturbed areas, indicating a slightly lower surface area. If this is a result of the spike in maximum values is however difficult to determine.

5.3.4 Differences between Seismic Line Types

The analysis of the different seismic line types revealed significant differences of the mean, between the older seismic lines, the newly cut lines and the re-disturbed lines. This is observed throughout all different quantification methods. The information revealed by these different quantification methods is however contradictory.

When analysing DTW the old seismic lines appear to have the greatest height maximums and have the highest average. The average distance to water however is very similar to the newly created lines. The newly created lines appear to suffer from a reduction of maximum DTW. This suggests that the microtopography on old seismic lines has not recovered very much on average, but maximum DTW has returned to the level of the surrounding fen.

The re-disturbed lines suffer from a notable reduction of mean height and maximum height. This suggests that re-disturbance might have a compounding effect on the depression of seismic lines. This could be a result of the repeated driving of heavy machinery.

Drawing conclusions from the moving window method is more difficult, as mean height does not vary much between lines. Bigger differences are observable between the ranges of newly created lines with 33 cm and a range of 38 cm on the re-disturbed and old seismic lines. For re-disturbed lines the range is a result of higher maximum values, while on old disturbed lines the higher range is a result of lower minimum values.

The same difficulty persists when analysing the SAR method, as mean values were judged to be significantly different, but are difficult to evaluate. The highest mean value 1.13 was recorded for newly disturbed lines, while old disturbed lines recorded a smaller mean with a mean of 1.12 and re-disturbed measured 1.11. This would suggest the microtopography is highest on newly created seismic lines.

The SAR and Moving Window methods are more affected by microtopography on the side of the lines, which may create noise. DTW is much less affected by the surrounding environment, and therefore may create more reliable results, when analysing small scale variation.

5.3.5 Applicability of Quantification Methods

When assessing the microtopography of an area, it is essential to consider various factors that can influence the results. Each method employed in this quantification process possesses its own set of advantages and limitations. Limiting this comparison is the relatively small amount of validation data for all quantification workflows.

The DTW method stands out, as the DTW is the most fundamental variable to explaining seedling survival. It provides researchers and restoration managers with an easily understandable metric that allows them to determine greenhouse gas emissions and specific

plant growth limitations linked to the water table. Therefore, allowing a more thorough analysis of the effects by disturbance. It is not affected as much by the surrounding microtopography and is therefore more useful when analysing smaller sample groups, as done in chapter 4.2. The methodology is however in its current state limited in its application to fen wetlands with a relatively low gradient. However, the workflow to determine DTW has the potential to be refined further (more in chapter 5.3.6). If the accuracy of this method remains satisfactory using the lower resolution airborne LiDAR still remains to be tested. If successfully tested this method would enable large scale surveys on the impact of seismic line disturbance in wetland areas.

The microform classification method using the local average has the advantage of being applicable in more sloped areas and will be able to capture variation between the surrounding of the seismic lines and seismic lines. It might therefore be especially useful when measuring disturbance in slightly sloped contexts such as bogs and upland areas, while still producing useful results in fen areas.

The SAR largely reflects the results of the other methods but appears more susceptible to faulty measurements. It is important to note that the SAR method was tested throughout more challenging environments, therefore limiting the comparison to the other methods. The values generated by this method are also more difficult to analyse by other researchers. It therefore might not be useful when comparing seismic lines to their surroundings. It however might be useful in the context of restoration planning, as it has been shown by this study that low values generated by this method are generally reliable. Therefore, seismic lines with a low level of microtopography should be identifiable by the SAR methods.

5.3.6 Scaling the Workflows and Future Research Directions

The good accuracy of the aircraft LiDAR throughout all ecosites and line types, suggests that the quantification methods should be transferable to measure microtopography on bigger scales. The quality of the DTM at 50 cm might be too coarse to capture the surface variation in a hummock and hollow landscape, according to Stovall et al., 2019. Their findings suggest a steep drop off in the sensitivity of microtopographic at a pixel size of 50 cm. Their recommended pixel size for detection of hummocks and hollows was around 25 cm, which allowed for the ideal segmentation of features. Theoretically the point density of 30 points per m^2 of the aircraft-based LiDAR system, would allow for the production of higher resolution DTMs. The development a new processing workflow to convert the LiDAR point clouds into DTMs

however exceeded the scope of this thesis. Future research should therefore aim to adapt the workflows proposed in this thesis to higher resolution DTMs derived from the aircraft LiDAR.

The novel DTW workflow implemented in this thesis, still has considerable room for improvement, using the raw LiDAR point clouds and more sophisticated spatial interpolation methods. This could create smoother groundwater surfaces, potentially increasing its applicability to more sloped terrain and further increasing its accuracy. This could allow for large scale analysis of disturbances in wetland areas.

5.4 Potential Sources of Error

All data used in this study are subject to a variety of error sources during collection, processing, and analysis. Firstly, the RTK GNSS is prone to inaccuracies as a result of variations in satellite connectivity and radio linkages. These inaccuracies are often influenced by factors, such as canopy cover (Roosevelt, 2014). The heavy canopy encountered on some regenerated sites sometimes forced the repositioning of transects, which may introduce bias. Another potential source of error and variability lays in the measurement techniques employed among field staff. To minimize these errors, only measurements within an acceptable standard deviation were used. We also ensured uniformity in field personnel to curtail discrepancies in ground measurements.

The potential errors related to the LiDAR measurements, were discussed at length in chapter 5.1 and the associated uncertainties in the quantification methods in chapter 5.2.

The analysis of the fen area relied on shapefiles supplied by the FLM, these however will at times include parts of the surrounding area, likely reducing the difference between disturbed and undisturbed areas.

6 Conclusion

The overarching objective of this thesis was to determine a workflow that allowed for the quantification of microtopography via remote sensing. Within the broader objective, the first objective of this research was to evaluate the performance of the RPAS LiDAR dataset across different ecosites and seismic lines. This was achieved by studying the dataset's accuracy in various environmental conditions and correlating the variations with influential factors such as vegetation and ecosite type. The evaluation included a detailed comparison of the RPAS LiDAR dataset's performance with the aircraft-based LiDAR dataset collected during the same time period.

This analysis yields two key findings. Firstly, it reveals substantial differences between sites based on environmental conditions. More precisely it identifies slope and vegetation as major influencers on the dataset's accuracy, with more complex terrains and denser vegetation generally leading to less accurate measurements. Secondly, it reveals the superior performance of airborne LiDAR compared to RPAS LiDAR across different ecosites and vegetation stages, demonstrating its robustness and reliability.

The second objective of this study was to quantify microtopography, here the SAR emerged as a valuable tool for identifying seismic lines that require restoration. Yet, it was found to overestimate the surface area on regenerating lines and complex surface structures. The method of quantifying DTW proved very accurate at measuring the water table in fen areas but is limited in its applicability by the necessity of open water presence, high water tables, and low gradient terrains. Finally, the microform method effectively measures average hummock-hollow ranges in fen areas, but the presence of steeper slopes proved to lead to both over- and underestimation. This thesis finds that due to the substantial differences between quantification methods, the selection of the quantification method must be highly dependent on the goals of the study and the characteristics of the study area.

When applying these methods on a poor fen, it revealed that disturbed areas suffered from a significant depression of microforms and a reduction of mean DTW. Therefore, their ability to regenerate was likely weakened. The investigation of differences between newly constructed seismic lines, re-disturbed lines and old lines revealed significant differences, indicating that especially re-disturbed lines suffer from a depression of their microtopography.

The high quality of the aircraft-based LiDAR system in a wide variety of terrain suggests that the methodologies to quantify microtopography are likely scalable to the entire BERA study region. This would allow the detection of seismic lines with diminished microtopography and therefore allow better allocation of restoration practices such as mounding. Resulting from this would be cost savings, less unnecessary disruption of locations exhibiting robust microtopographic recovery and a reduction of greenhouse gas release.

References

AHFMP - A Historical Overview of Geophysical Exploration In Alberta, n.d.

Bater, C.W., Coops, N.C., 2009. Evaluating error associated with lidar-derived DEM interpolation. Comput. Geosci. 35, 289–300. https://doi.org/10.1016/j.cageo.2008.09.001

Branch, L.S., 2023. Consolidated federal laws of Canada, Species at Risk Act [WWW Document]. URL https://www.laws-lois.justice.gc.ca/eng/acts/S-15.3/ (accessed 6.19.23).

Bubier, J.L., Moore, T.R., Roulet, N.T., 1993. Methane Emissions from Wetlands in the Midboreal Region of Northern Ontario, Canada. Ecology 74, 2240–2254. https://doi.org/10.2307/1939577

Canada, E. and C.C., 2013. Canadian Climate Normals 1981-2010 Station Data - Climate - Environment and Climate Change Canada [WWW Document]. URL https://climate.weather.gc.ca/climate_normals/results_1981_2010_e.html?searchType=stnName&txtStationName=Fort+McMurray&searchMethod=contains&txtCentralLatMin=0&txtCentralLatSec=0&txtCentralLongMin=0&txtCentralLongSec=0&stnID=2519&dispBack=1 (accessed 4.28.23).

Caners, R.T., Lieffers, V.J., 2014. Divergent Pathways of Successional Recovery for In Situ Oil Sands Exploration Drilling Pads on Wooded Moderate-Rich Fens in Alberta, Canada. Restor. Ecol. 22, 657–667. https://doi.org/10.1111/rec.12123

Chisholm, R.A., Cui, J., Lum, S.K.Y., Chen, B.M., 2013. UAV LiDAR for below-canopy forest surveys. J. Unmanned Veh. Syst. 01, 61–68. https://doi.org/10.1139/juvs-2013-0017

Cresto Aleina, F., Runkle, B.R.K., Brücher, T., Kleinen, T., Brovkin, V., 2016. Upscaling methane emission hotspots in boreal peatlands. Geosci. Model Dev. 9, 915–926. https://doi.org/10.5194/gmd-9-915-2016

Dabros, A., Pyper, M., Castilla, G., 2018. Seismic lines in the boreal and arctic ecosystems of North America: environmental impacts, challenges, and opportunities. Environ. Rev. 26, 214–229. https://doi.org/10.1139/er-2017-0080

De Roos, S., Turner, D., Lucieer, A., Bowman, D.M.J.S., 2018. Using Digital Surface Models from UAS Imagery of Fire Damaged Sphagnum Peatlands for Monitoring and Hydrological Restoration. Drones 2, 45. https://doi.org/10.3390/drones2040045

Echiverri, L.F.I., Macdonald, S.E., Nielsen, S.E., 2022. Neighboring edges: Interacting edge effects from linear disturbances in treed fens. Appl. Veg. Sci. 25, e12645. https://doi.org/10.1111/avsc.12645

Eppinga, M.B., de Ruiter, P.C., Wassen, M.J., Rietkerk, M., 2009. Nutrients and Hydrology Indicate the Driving Mechanisms of Peatland Surface Patterning. Am. Nat. 173, 803–818. https://doi.org/10.1086/598487

Erdody, T.L., Moskal, L.M., 2010. Fusion of LiDAR and imagery for estimating forest canopy fuels. Remote Sens. Environ. 114, 725–737. https://doi.org/10.1016/j.rse.2009.11.002

Filicetti, A.T., Cody, M., Nielsen, S.E., 2019. Caribou Conservation: Restoring Trees on Seismic Lines in Alberta, Canada. Forests 10, 185. https://doi.org/10.3390/f10020185

Fritz, A., Kattenborn, T., Koch, B., 2013. UAV-BASED PHOTOGRAMMETRIC POINT CLOUDS – TREE STEM MAPPING IN OPEN STANDS IN COMPARISON TO TERRESTRIAL LASER SCANNER POINT CLOUDS. Int. Arch. Photogramm. Remote Sens. Spat. Inf. Sci. XL-1-W2, 141–146. https://doi.org/10.5194/isprsarchives-XL-1-W2-141-2013

Hebblewhite, M., 2017. Billion dollar boreal woodland caribou and the biodiversity impacts of the global oil and gas industry. Biol. Conserv. 206, 102–111. https://doi.org/10.1016/j.biocon.2016.12.014

Hogg, E.H., 1993. Decay Potential of Hummock and Hollow Sphagnum peats at Different Depths in a Swedish Raised Bog. Oikos 66, 269–278. https://doi.org/10.2307/3544814

Holmquist, J.R., MacDonald, G.M., Gallego-Sala, A., 2014. Peatland Initiation, Carbon Accumulation, and 2 ka Depth in the James Bay Lowland and Adjacent Regions. Arct. Antarct. Alp. Res. 46, 19–39.

Jenness, J.S., 2004. Calculating landscape surface area from digital elevation models. Wildl. Soc. Bull. 32, 829–839. https://doi.org/10.2193/0091-7648(2004)032[0829:CLSAFD]2.0.CO;2
Johnson, E.A., Miyanishi, K., 2008. Creating new landscapes and ecosystems: the Alberta Oil Sands. Ann. N. Y. Acad. Sci. 1134, 120–145. https://doi.org/10.1196/annals.1439.007
Lapointe, R., Langor, D., Dabros, A., Pinno, B., Spence, J., Pyper, M., Hirsch, K., 2015. Science-based responsible resource development: Lessons learned from two Canadian success stories.
Latham, A.D.M., Latham, M.C., Boyce, M.S., Boutin, S., 2011. Movement responses by wolves to industrial linear features and their effect on woodland caribou in northeastern Alberta. Ecol. Appl. 21, 2854–2865. https://doi.org/10.1890/11-0666.1
Lee, P., Boutin, S., 2006. Persistence and developmental transition of wide seismic lines in the western Boreal Plains of Canada. J. Environ. Manage. 78, 240–250. https://doi.org/10.1016/j.jenvman.2005.03.016
Lehmann, J.R.K., Münchberger, W., Knoth, C., Blodau, C., Nieberding, F., Prinz, T., Pancotto, V.A., Kleinebecker, T., 2016. High-Resolution Classification of South Patagonian Peat Bog Microforms Reveals Potential Gaps in Up-Scaled CH4 Fluxes by use of Unmanned Aerial System (UAS) and CIR Imagery. Remote Sens. 8, 173. https://doi.org/10.3390/rs8030173
Lieffers, V.J., Rothwell, R.L., 1987. Effects of drainage on substrate temperature and phenology of some trees and shrubs in an Alberta peatland. Can. J. For. Res. 17, 97–104. https://doi.org/10.1139/x87-019
Lindsay, J.B., 2016. Whitebox GAT: A case study in geomorphometric analysis. Comput. Geosci. 95, 75–84. https://doi.org/10.1016/j.cageo.2016.07.003
Linke, J., G.J McDermid, C. Shellian, S.E. Nielsen, C. Sutheimer, S. Ketcheson, M. Strack and E. Bayne., 2022. BERA Field Protocols: Site Assessment and Inventory for Linear Human Footprint Features.
Lovitt, J., Rahman, M.M., McDermid, G.J., 2017. Assessing the Value of UAV Photogrammetry for Characterizing Terrain in Complex Peatlands. Remote Sens. 9, 715. https://doi.org/10.3390/rs9070715
Lovitt, J., Rahman, M.M., Saraswati, S., McDermid, G.J., Strack, M., Xu, B., 2018. UAV Remote Sensing Can Reveal the Effects of Low-Impact Seismic Lines on Surface Morphology, Hydrology, and Methane (CH4) Release in a Boreal Treed Bog. J. Geophys. Res. Biogeosciences 123, 1117–1129. https://doi.org/10.1002/2017JG004232
Mancini, F., Dubbini, M., Gattelli, M., Stecchi, F., Fabbri, S., Gabbianelli, G., 2013. Using Unmanned Aerial Vehicles (UAV) for High-Resolution Reconstruction of Topography: The Structure from Motion Approach on Coastal Environments. Remote Sens. 5, 6880–6898. https://doi.org/10.3390/rs5126880
Moudrý, V., Klápště, P., Fogl, M., Gdulová, K., Barták, V., Urban, R., 2020. Assessment of LiDAR ground filtering algorithms for determining ground surface of non-natural terrain overgrown with forest and steppe vegetation. Measurement 150, 107047. https://doi.org/10.1016/j.measurement.2019.107047
Nelson, K., Chasmer, L., Hopkinson, C., 2022. Quantifying Lidar Elevation Accuracy: Parameterization and Wavelength Selection for Optimal Ground Classifications Based on Time since Fire/Disturbance. Remote Sens. 14, 5080. https://doi.org/10.3390/rs14205080
Price, D.T., Alfaro, R.I., Brown, K.J., Flannigan, M.D., Fleming, R.A., Hogg, E.H., Girardin, M.P., Lakusta, T., Johnston, M., McKenney, D.W., Pedlar, J.H., Stratton, T., Sturrock, R.N., Thompson, I.D., Trofymow, J.A., Venier, L.A., 2013. Anticipating the consequences of climate change for Canada's boreal forest ecosystems. Environ. Rev. 21, 322–365. https://doi.org/10.1139/er-2013-0042
Pyper, M., Nishi, J., McNeil, L., 2014. Linear Feature Restoration in Caribou Habitat: A summary of current practices and a roadmap for future programs. https://doi.org/10.13140/RG.2.1.3958.3766

Rahman, M.M., McDermid, G.J., Strack, M., Lovitt, J., 2017. A New Method to Map Groundwater Table in Peatlands Using Unmanned Aerial Vehicles. Remote Sens. 9, 1057. https://doi.org/10.3390/rs9101057

Riley, S., Degloria, S., Elliot, S.D., 1999. A Terrain Ruggedness Index that Quantifies Topographic Heterogeneity. Int. J. Sci. 5, 23–27.

Roosevelt, C., 2014. Roosevelt 2014: Mapping site-level Microtopography with Real-Time Kinematic Global Navigation Satellite Systems (RTK GNSS) and Unmanned Aerial Vehicle Photogrammetry (UAVP). Open Archaeol.

Schmidt, M., Davidson, S.J., Strack, M., 2022. CO2 uptake decreased and CH4 emissions increased in first two years of peatland seismic line restoration. Wetl. Ecol. Manag. 30, 313–329. https://doi.org/10.1007/s11273-022-09858-4

Stern, E.R., Riva, F., Nielsen, S.E., 2018. Effects of Narrow Linear Disturbances on Light and Wind Patterns in Fragmented Boreal Forests in Northeastern Alberta. Forests 9, 486. https://doi.org/10.3390/f9080486

Stevenson, C., Filicetti, A., Nielsen, S., 2019. High Precision Altimeter Demonstrates Simplification and Depression of Microtopography on Seismic Lines in Treed Peatlands. Forests 10, 295. https://doi.org/10.3390/f10040295

Stovall, A.E.L., Diamond, J.S., Slesak, R.A., McLaughlin, D.L., Shugart, H., 2019. Quantifying wetland microtopography with terrestrial laser scanning. Remote Sens. Environ. 232, 111271. https://doi.org/10.1016/j.rse.2019.111271

Strack, M., 2008. Peatlands and Climate Change. IPS, International Peat Society.

Strack, M., Hayne, S., Lovitt, J., McDermid, G.J., Rahman, M.M., Saraswati, S., Xu, B., 2019. Petroleum exploration increases methane emissions from northern peatlands. Nat. Commun. 10, 2804. https://doi.org/10.1038/s41467-019-10762-4

Sutton, R.F., 1993. Mounding site preparation: A review of European and North American experience. New For. 7, 151–192. https://doi.org/10.1007/BF00034198

van Rensen, C.K., Nielsen, S.E., White, B., Vinge, T., Lieffers, V.J., 2015. Natural regeneration of forest vegetation on legacy seismic lines in boreal habitats in Alberta's oil sands region. Biol. Conserv. 184, 127–135. https://doi.org/10.1016/j.biocon.2015.01.020

Westoby, M.J., Brasington, J., Glasser, N.F., Hambrey, M.J., Reynolds, J.M., 2012. 'Structure-from-Motion' photogrammetry: A low-cost, effective tool for geoscience applications. Geomorphology 179, 300–314. https://doi.org/10.1016/j.geomorph.2012.08.021

Zenmuse_L1 _User Manual_DE_v1.2.pdf, n.d.

Zolkos, S.G., Goetz, S.J., Dubayah, R., 2013. A meta-analysis of terrestrial aboveground biomass estimation using lidar remote sensing. Remote Sens. Environ. 128, 289–298. https://doi.org/10.1016/j.rse.2012.10.017

Appendix

LiDAR Workflow

Down below is the code used to process the LiDAR dataset. The first code preprocesses the point cloud, to get rid of a diverse range of artefacts, encountered during the processing. The second part of the code calculated in R thins the points down to a uniform 147 points per m^2. The third part of the code classifies the ground and creates the input for the DTM generation conducted in ArcGISpro.

```
@ echo off
:: Batch script for preprocessing LiDAR data to prepare the creation of DEM,
DSM, and CHM
:: 0. Metadata
:: - lasvalidate Verify validity of the dataset
:: - lasindex
:: - lasinfo
:: - lasgrid
:: 1. Flightline cleansing
:: - lasclip
can be separated
:: - lassplit
:: - lasoverlap

flightlines and height difference
Create a spatial index
Metadata
Generate point density raster
Clip flightlines to flight boundaries so flightlines
Divide file into flightlines based on GPS-time gaps
Generate raster respectively with the amount of

:: - lasoverage
:: 2. Data cleansing
:: - lastile
:: - lasduplicate
:: - lasnoise
:: Author: Jasper Koch, Marlis Hegels
:: Munich, February 2023

REM ::::::::::::::
REM :: Set paths ::
REM ::::::::::::::

:: sets the path to the folder that stores the las binary files
SET PATH=%PATH%;C:\Users\marlis.hegels\Desktop\LAStools\bin;
:: sets the path to raw lidar folder
set RAW_LIDAR=N:\KirbySouth_L1_Summer2022\output_las
:: sets the path to the flight areas folder
set AREAS=N:\Flightareas
:: set the path to the folder that will contain the results and the raw file
set FILES=N:\KirbySouth2022_preprocessed

REM ::::::::::::::::::
REM :: Set parameters ::
REM ::::::::::::::::::

set CORES=30
REM lasgrid
set STEP_PD_GRID=1
set PD_GRID=100
REM lassplit
set TIME_GAP=0.1
```

```
REM lastile
set TILE_SIZE=60
set TILE_BUFFER=5
REM lasnoise
set STEP_XY=1
set STEP_Z=1
set POINTS=20
set SA=32
echo Parameter settings:
echo %CORES%     - Cores
echo %STEP_PD_GRID%
echo %PD_GRID%   - lasgrid: grid size for point density raster in centimeter
echo %TIME_GAP% - lassplit: GPS-time gap to separate flightlines

echo %TILE_SIZE% - lastile: tile_size
echo %TILE_BUFFER% - lastile: buffer

echo %STEP_XY%
echo %STEP_Z%
echo %POINTS%
echo %SA%

- lasnoise: step_xy
- lasnoise: step_z
- lasnoise: isolated
- lasnoise: maximum scan angle
- lasgrid: grid size for point density raster in meter
:: For each las file in the RAW_LIDAR folder
SETLOCAL ENABLEDELAYEDEXPANSION
for /r "%RAW_LIDAR%" %%i in (*.las) do (

 REM ::::::::::::::::::::
      REM :: Manage variables ::
      REM ::::::::::::::::::::
      :: file path of input raw LiDAR file
      set FP=%%i
      echo !FP!
      :: file name w\ extension
      REM echo %%~nxi
      :: file name w\o extension
      set FN=%%~ni
      echo !FN!
      :: area letter
      set AREA=%%~ni
      set AREA=!AREA:~-1,1!
      echo !AREA!

      REM :::::::::::::::::::::::
      REM :: Manage file paths ::
      REM :::::::::::::::::::::::

      :: create an output folder
      if exist %FILES%\!FN! rmdir /s /q %FILES%\!FN!
      mkdir %FILES%\!FN!
      :: create folder structure
      mkdir %FILES%\!FN!\00_Info
      mkdir %FILES%\!FN!\01_Clip
      mkdir %FILES%\!FN!\02_Flightlines
      mkdir %FILES%\!FN!\03_CleanedFlightlines
      mkdir %FILES%\!FN!\03_FlightlineRaster
      mkdir %FILES%\!FN!\04_Tiles
      mkdir %FILES%\!FN!\05_NoDups
      mkdir %FILES%\!FN!\06_Noise

REM ::::::::::::::::::::
REM :: START COMPUTING ::
```

```
REM ::::::::::::::::::::
echo %date% %time%
:: 0. Metadata
- Start computing

:: 0.1 Verify the validity
lasvalidate -i !FP! ^
-o %FILES%\!FN!\00_Info\validate.xml
echo %date% %time% - lasvalidate done

:: 0.2 Spatial index of input las-file lasindex -i !FP! -dont_reindex
echo %date% %time% - lasindex done

:: 0.3 Metadata txt-file
lasinfo -i !FP! ^
-cd -histo scan_angle 1 ^
-odir %FILES%\!FN!\00_Info -odix _INFO -otxt echo %date% %time% - lasinfo done

:: 0.4 Generate point density raster
lasgrid -i !FP! -last_only ^
-density -step %STEP_PD_GRID% ^
-use_bb -nad83 -utm 12U ^

-odir %FILES%\!FN!\00_Info -odix _PD%PD_GRID%cm -oasc echo %date% %time% - lasgrid done

:: 1. Flightline cleansing
:: 1.1 Clip LAS file with flight line shape file so flightiness can be :: separated
lasclip -i !FP! ^
-poly %AREAS%\!AREA!.shp ^
-odir %FILES%\!FN!\01_Clip -olaz
echo %date% %time% - lasclip done

:: 1.2 Divide the flightlines based on GPS time
lassplit -i %FILES%\!FN!\01_Clip\*.laz ^
-recover_flightlines_interval %TIME_GAP% ^
-odir %FILES%\!FN!\02_Flightlines -olaz

echo %date% %time% - lassplit done

:: 1.3 Generate a raster with the amount of flightlines and height
:: difference
lasoverlap -i %FILES%\!FN!\02_Flightlines\*.laz ^
-merged -faf -step %STEP_PD_GRID% ^

-values -elevation -lowest ^
-nad83 -utm 12U ^
-odir %FILES%\!FN!\03_FlightlineRaster -oasc echo %date% %time% - lasoverlap done

:: 1.4 Delete overlapping points
lasoverage -i %FILES%\!FN!\02_Flightlines\*.laz ^ -faf -remove_overage -merged ^
-odir %Files%\!FN!\03_CleanedFlightlines -olaz echo %date% %time% - lasoverage done

:: 1.5 Generate point density raster
lasgrid -i %Files%\!FN!\03_CleanedFlightlines\*.laz -last_only ^ -density -step %STEP_PD_GRID% ^
-use_bb -nad83 -utm 12U ^
-odir %FILES%\!FN!\03_FlightlineRaster -odix _PD%PD_GRID%cm -oasc echo %date% %time% - lasgrid done

:: 2. Data cleansing
:: 2.1 Make data manageable by creating files that are easier to :: compute
lastile -i %FILES%\!FN!\03_CleanedFlightlines\*.laz ^
-tile_size %TILE_SIZE% -buffer %TILE_BUFFER% -flag_as_synthetic ^ -odir %FILES%\!FN!\04_Tiles -olaz
echo %date% %time% - lastile done
```

```
:: 2.2 Delete duplicates
lasduplicate -i %FILES%\!FN!\04_Tiles\*.laz ^


-unique_xyz ^
-cores %CORES% ^
-odir %FILES%\!FN!\05_NoDups -olaz
echo %date% %time% - lasduplicate done

:: 2.3 Classify noise
lasnoise -i %FILES%\!FN!\05_NoDups\*.laz ^ -step_xy %STEP_XY% -step_z %STEP_Z% ^
-isolated %POINTS% -keep_scan_angle -%SA% %SA% ^ -cores %CORES% ^
-odir %FILES%\!FN!\06_Noise -olaz
echo %date% %time% - lasnoise done

      REM ::::::::::::::::::::::::::
      REM :: Delete intermediates ::
      REM ::::::::::::::::::::::::::
      :: remove output folder
      rmdir /s /q %FILES%\!FN!\01_Clip
      rmdir /s /q %FILES%\!FN!\02_Flightlines
      rmdir /s /q %FILES%\!FN!\03_CleanedFlightlines
      rmdir /s /q %FILES%\!FN!\04_Tiles
      rmdir /s /q %FILES%\!FN!\05_NoDups

echo %date% %time% - !AREA! done

)
echo %date% %time% - Clean all done pause
```

A.5.2 R script for point density homogenization

```
# Code by Marlis Hegels
# Purpose:
# Thin LiDAR tiles to a certain point density based on pulses
library(lidR)
library(future)
library(comprehenr)
# settings ---------------------------------------

setwd("N:/KirbySouth2022_preprocessed")
las_raw = "N:/KirbySouth_L1_Summer2022/output_las"
pd=147 #achieved point density
res_thinning = 1 # pixel size used to filter the points
input_folder = "06_Noise"
output_folder = paste("07_ThinnedPD", as.character(pd), sep="")
areas = list.files(las_raw, pattern = "\\.las")
areas = to_vec(for (area in areas) substr(area,1,16))

for (area in areas) {
  # create an output folder
  dir.create(paste(area, "/", output_folder, sep=""), showWarnings = F)
  # Delete all files in the output folder
  unlink(paste(area, "/", output_folder, "/*", sep=""))
  # for every tile
  filenames = list.files(paste(area, "/", input_folder, "/", sep=""))
  for(file in filenames) {
    cat(area, file, "\n")
    las = readLAS(paste(area, "/", input_folder, "/", file, sep=""))
    las = retrieve_pulses(las)
    thinned = decimate_points(las, homogenize(pd,res_thinning,use_pulse = T))
    density = rasterize_density(thinned, res=1)
    plot(density)
    writeLAS(thinned, paste(area, "/", output_folder, "/", file, sep=""))
```

A.5.3 Batch script for LAStools to classify points

```
@ echo off
:: Batch script for preprocessing LiDAR data to prepare the creation of DEM, DSM, and CHM
:: 3. Classifying
:: - lasground
:: - lasthin
:: - lasclassify
:: - lasheight
:: - lasclassify
:: 4. Merging
:: - lasmerge
:: 5. Metadata preprocessed output
:: - lasinfo Metadata
:: - lasindex Generate spatial index
:: Author: Jasper Koch, Marlis Hegels
:: Munich, February 2023

REM ::::::::::::::
REM :: Set paths ::
REM ::::::::::::::

:: sets the path to the folder that stores the las binary files
SET PATH=%PATH%;C:\Users\marlis.hegels\Desktop\LAStools\bin;
:: sets the path to raw lidar folder
set RAW_LIDAR=N:\KirbySouth_L1_Summer2022\output_las
:: sets the path to the flight areas folder
set AREAS=N:\Flightareas
:: set the path to the folder that will contain the results and the raw file
set FILES=N:\KirbySouth2022_preprocessed

REM ::::::::::::::::::
REM :: Set parameters ::
REM ::::::::::::::::::

set CORES=30
REM lasthin
set PD=147
set STEP_T=0.1
REM lasground
set STEP_G=3
set OFFSET_G=0.1
REM lasclassify
set OFFSET_C=1.0
echo Parameter settings:
echo %CORES%
echo %PD%
echo %STEP_T%
echo %STEP_G%
echo %OFFSET_G%  - lasground: offset
echo %OFFSET_C%  - lasclassify: ground_offset

Classify ground
Thin ground points
Reclassify thinned points to ground points
Calculate point height over the ground
Classify points >1m over the ground as high vegetation

Merge files

- Cores
- lasthin: max. point density
- lasthin: step
- lasground: step
```

```
:: For each las file in the RAW_LIDAR folder
SETLOCAL ENABLEDELAYEDEXPANSION
for /r "%RAW_LIDAR%" %%i in (*.las) do (


	REM ::::::::::::::::::::::
	REM :: Manage variables ::
	REM ::::::::::::::::::::::

:: file path of input raw LiDAR file
set FP=%%i
echo !FP!
:: file name w\ extension
REM echo %%~nxi
:: file name w\o extension
set FN=%%~ni
echo !FN!
:: area letter
set AREA=%%~ni
set AREA=!AREA:~-1,1!
echo !AREA!
REM ::::::::::::::::::::::
REM :: Manage file paths ::
REM ::::::::::::::::::::::

:: create folder structure
mkdir %FILES%\!FN!\08_Ground
mkdir %FILES%\!FN!\09_GroundThinned
mkdir %FILES%\!FN!\10_Classified
mkdir %FILES%\!FN!\11_Height
mkdir %FILES%\!FN!\12_Reclassified
mkdir %FILES%\!FN!\13_Merged
mkdir %FILES%\!FN!\14_Raster
REM ::::::::::::::::::::
REM :: START COMPUTING ::
REM ::::::::::::::::::::
echo %date% %time%
- Start computing

:: 3. Classifying
:: 3.1 Classify ground
lasground -i %FILES%\!FN!\07_ThinnedPD%PD%\*.laz ^ -compute_height -ignore_class 7 ^
-step %STEP_G% -offset %OFFSET_G% ^
-cores %CORES% ^
-odir %FILES%\!FN!\08_Ground -olaz
echo %date% %time% - lasground done

:: 3.2 Thin ground
lasthin -i %FILES%\!FN!\08_Ground\*.laz ^ -ignore_class 1 -classify_as 14 ^
-lowest -step %STEP_T% ^
-cores %CORES% ^
-odir %FILES%\!FN!\09_GroundThinned -olaz
echo %date% %time% - lasthin ground done

:: 3.3 Reclassify thinned points to ground points
lasclassify -i %FILES%\!FN!\09_GroundThinned\*.laz ^
-change_classification_from_to 2 13 ^
-change_classification_from_to 14 2 ^

-cores %CORES% ^
-odir %FILES%\!FN!\10_Classified -olaz
echo %date% %time% - lasclassify thinned ground done

:: 3.4 Recalculate point height above ground
lasheight -i %FILES%\!FN!\10_Classified\*.laz ^
```

```
-cores %CORES% ^
-odir %FILES%\!FN!\11_Height -olaz

echo %date% %time% - lasheight done

:: 3.5 Classify points 1 meter  above the ground as high vegetation
lasclassify -i %FILES%\!FN!\11_Height\*.laz ^
-ground_offset %OFFSET_C% -small_trees ^
-cores %CORES% ^
-odir %FILES%\!FN!\12_Reclassified -olaz

echo %date% %time% - lasclassify high vegetation done

:: 4 Merging the file
lasmerge -i %FILES%\!FN!\12_Reclassified\*.laz ^ -drop_synthetic ^
-o %FILES%\!FN!\13_Merged\!FN!_PD%PD%.las
echo %date% %time% - lasmerge done

:: 4.1 Spatial index of output las-file
lasindex -i %FILES%\!FN!\13_Merged\!FN!_PD%PD%.las -dont_reindex echo %date% %time% - lasindex done

:: 5. Metadata preprocessed output
:: 5.1 Compute Metadata
lasinfo -i %FILES%\!FN!\13_Merged\!FN!_PD%PD%.las ^ -cd -histo scan_angle 1 ^
-odir %FILES%\!FN!\13_Merged -odix _INFO -otxt
echo %date% %time% - lasinfo done

REM ::::::::::::::::::::::::
REM :: Delete intermediates ::
REM ::::::::::::::::::::::::
:: remove output folder
rmdir /s /q %FILES%\!FN!\08_Ground
rmdir /s /q %FILES%\!FN!\09_GroundThinned
rmdir /s /q %FILES%\!FN!\10_Classified
rmdir /s /q %FILES%\!FN!\11_Height

echo %date% %time% - !AREA! done

echo %date% %time% - Classify all done pause
```

ERKLÄRUNG

Hiermit erkläre ich, dass ich die vorliegende Arbeit selbständig verfasst habe, noch nicht anderweitig für Prüfungszwecke vorgelegt, keine anderen als die angegebenen Quellen oder Hilfsmittel benutzt, sowie Zitate als solche gekennzeichnet habe.

München, 17.06.2023

.....

(Jasper Koch)